NASA CR-72745
GA-10194

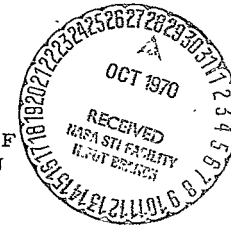

FINAL REPORT

NEUTRON CAPTURE CROSS SECTIONS OF MOLYBDENUM, TANTALUM, AND ^{238}U

by

S. J. Friesenhahn, W. M. Lopez, M. P. Fricke
D. G. Costello and A. D. Carlson

GULF GENERAL ATOMIC

prepared for

NATIONAL AERONAUTICS AND SPACE ADMINISTRATION

NASA Lewis Research Center
Contract NAS 3-11844
Sam Barile, Project Manager

NOTICE

This report was prepared as an account of Government-sponsored work. Neither the United States, nor the National Aeronautics and Space Administration (NASA), nor any person acting on behalf of NASA:

A.) Makes any warranty or representation, expressed or implied, with respect to the accuracy, completeness, or usefulness of the information contained in this report, or that the use of any information, apparatus, method or process disclosed in this report may not infringe privately owned rights; or

B.) Assumes any liabilities with respect to the use of, or for damages resulting from the use of, any information, apparatus, method or process disclosed in this report.

As used above, "person acting on behalf of NASA" includes any employee or contractor of NASA, or employee of such contractor, to the extent that such employee or contractor of NASA, or employee of such contractor, prepares, disseminates, or provides access to, any information pursuant to his employment or contract with NASA, or his employment with such contractor.

Requests for copies of this report should be referred to:

National Aeronautics and Space Administration
Office of Scientific and Technical Information
Attention: AFSS-A
Washington, D. C. 20546

NASA CR-72745
GA-10194

FINAL REPORT

NEUTRON CAPTURE CROSS SECTIONS OF MOLYBDENUM, TANTALUM, AND ^{238}U

by

S. J. Friesenhahn, W. M. Lopez, M. P. Fricke,
D. G. Costello and A. D. Carlson

GULF GENERAL ATOMIC
P. O. Box 608
San Diego, California 92112

prepared for

NATIONAL AERONAUTICS AND SPACE ADMINISTRATION

June 5, 1970

CONTRACT NAS 3-11844

Technical Management
NASA Lewis Research Center
Cleveland, Ohio
Nuclear Systems Division
Sam Barile, Project Manager
John C. Liwosz, Jr.

ABSTRACT

Absolute neutron capture cross sections for natural molybdenum, tantalum, and ^{238}U were measured from $\sim$ 1 to 1000 keV energy using the time-of-flight technique. The neutron flux spectrum was monitored with ^{3}He proportional counters that were calibrated against measurements based on the $^{10}B(n,\alpha)^{7}Li$ cross section below 80 keV and on the n+p scattering cross section at higher energies. The measured energy variation of the capture cross sections above 80 keV relies solely upon the n+p cross section; the cross sections are normalized directly to resolved resonances at low (eV) energies.

SUMMARY

Absolute neutron capture cross sections for natural molybdenum, tantalum, and the isotope ^{238}U were measured at continuous neutron energy intervals over the region ~ 1 to 1000 keV using an electron LINAC pulsed neutron source, a 230-meter neutron flight path and a large liquid scintillator to detect capture gamma rays. No previous measurement of any capture cross section has spanned the full energy range covered here, and previous measurements with electron LINACs have all been confined to energies below 200 keV.

The Ta and ^{238}U cross sections were normalized by the saturated-resonance technique, and the molybdenum cross section was normalized to low-energy resonance areas. The overall uncertainties (including both absolute and relative errors) of the Ta and ^{238}U cross sections are 10-15% at all energies. A higher overall uncertainty (~30%) is present for the molybdenum cross section, which is due primarily to large uncertainties in existing resonance-parameter information.

The incident neutron flux was monitored by ^{3}He gas proportional counters whose response for different neutron energies had been calibrated against that of other counters containing BF_3 and methane gas. The methane counter was also used to directly determine the flux at energies above 80 keV. The measured energy variation of the neutron flux, and hence the capture cross sections, is thus based on the cross section for the $^{10}B(n,\alpha)^{7}Li$ reaction for neutron energies below 80 keV and on the n+p scattering cross section at higher energies. The energy dependence of the neutron flux was thus determined with an uncertainty of < 5% over the full energy range of the capture measurements.

Measurements of neutron flux with the methane counter were accomplished with a computer-based, on-line data acquisition system which permits a correlation of neutron flight time and proton-recoil energy. Since the proton energy spectrum varies with the neutron energy, such data are necessary to determine the efficiency of the counter (which varies with neutron energy for a fixed electronic threshold).

CONTENTS

ILLUSTRATIONS

ILLUSTRATIONS (Continued)

This new capture gamma-ray detector achieves a much improved signal-to-background ratio and thus improves the accuracy and reliability of the capture data. To our knowledge, this installation is unique in its combination of a high-efficiency gamma-ray detector with a very long flight path. The excellent capture gamma-ray summing properties of this new detector along with its coincidence detection capabilities reduce background levels dramatically. This improved detector was essential in the measurement of $^{238}U(n, \gamma)$.

In the following sections we describe the experimental facility, the detectors employed in the measurements, the procedures used in data acquisition, the results of the data analysis, and conclusions drawn from the measurements. An appendix containing two papers concerning this work is attached. They have been accepted for presentation at the IAEA Second International Conference on Nuclear Data for Reactors, Helsinki, Finland, June 15-19, 1970.

2. EXPERIMENTAL FACILITY

2.1 NEUTRON SOURCE

The Gulf General Atomic linear accelerator is used to generate short bursts of photoneutrons by bombarding a small tungsten-alloy target with a 45-MeV electron beam. The target is surrounded by a cylindrical ^{238}U shield which serves the dual purpose of absorbing bremsstrahlung radiation and degrading the primary neutron energy spectrum by inelastic scattering.

To increase the number of low-energy neutrons, a 2.54-cm-thick slab of polyethylene is placed adjacent to the uranium and perpendicular to the flight path, as shown in Fig. 1. The polyethylene slab has the added advantages of reducing the slowing-down time spread and removing fine structure in the flux spectrum. The polyethylene is effective in modifying the neutron spectrum for all neutron energies at which the slab is at least one mean free path thick, i.e. $E_n \leq 500$ keV. For these neutron energies the resolution width contribution due to slowing-down time spread is approximately that resulting from the polyethylene, i.e. $\frac{\Delta E}{E} = 1.4 \times 10^{-4}$ and for $E_n \geq 500$ keV the effective time spread is approximately the mean neutron lifetime in the ^{238}U cylinder, i.e. $\frac{\Delta E}{E} = 8 \times 10^{-4}$.

2.2 220-METER FLIGHT PATH

An aerial view of the 230-meter flight path is shown in Fig. 2. The flight path was designed to provide a large-diameter, well-collimated neutron beam with a minimum of small-angle scattering of neutrons and gamma rays. Materials which introduce a significant amount of resonant structure in the neutron spectrum have been excluded from the beam path. This is achieved by evacuating the flight path and using thin

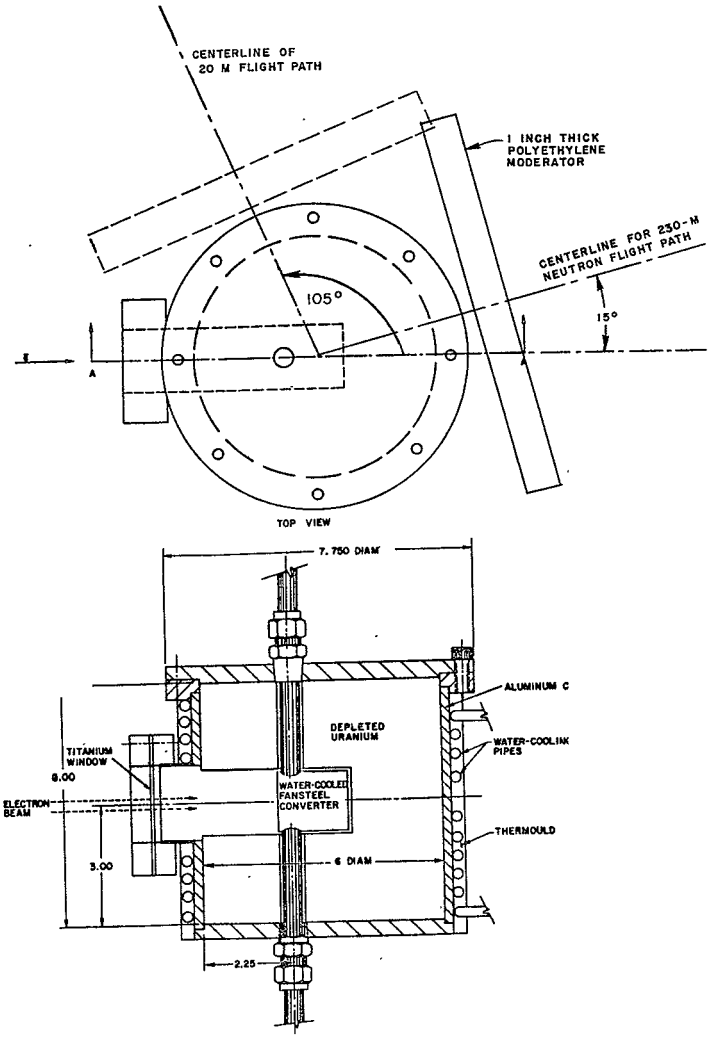

Fig. 1. Cross section view of uranium shielded electron target for neutron production.

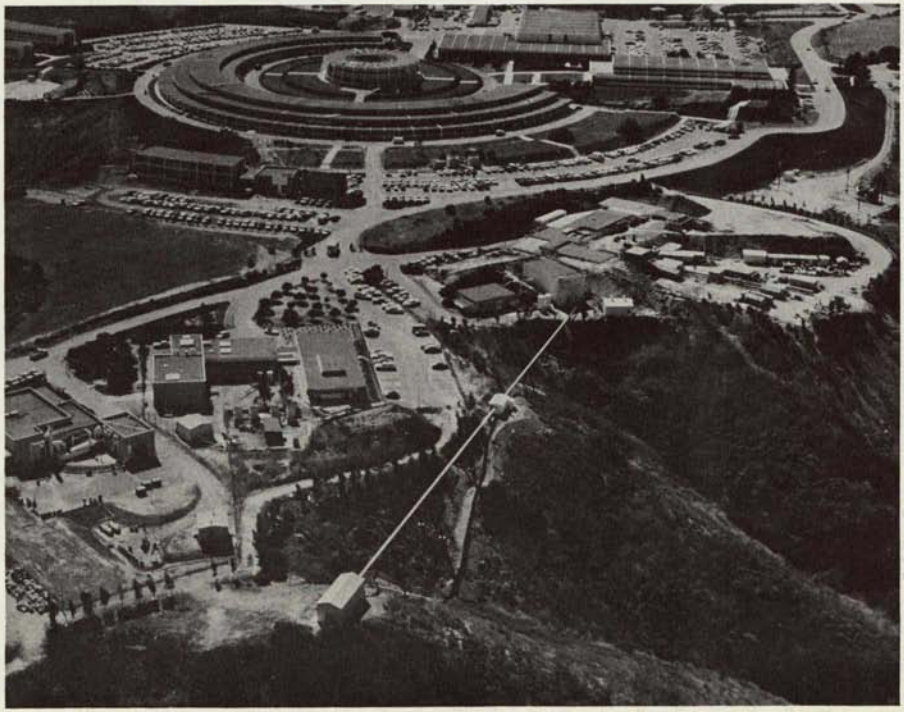

Fig. 2. Aerial view of the 230-meter flight path emerging from the Linac facility

Mylar exit windows. These precautions eliminate structure in the neutron flux which might otherwise be of significance when detectors with different timing properties are used in the same experiment.

During the contract year improvements in the vacuum system have increased the reliability of the flight-path vacuum. A resurvey of the flight-path elements confirmed the alignment stability of the structure and provided fiducial points for the placement of the 2400-liter scintillator described in Section 2.3.3.

It is necessary to filter low-energy neutrons out of the beam in order to allow operation of the LINAC at high repetition rates without overlap of adjacent bursts. A layer of ^{10}B powder (0.0116 atoms/barn), positioned at the entrance to the first collimator, was used for this purpose. In order to avoid undesirable scattering and absorption, which would result if a binder were used to hold the boron powder in place, a special evacuated holder for the powder was constructed. The holder consists of two 0.007-in. (0.0178-cm) Mylar sheets clamped on either side of a 0.1-in. (0.254-cm) brass spacer ring. A uniform layer of boron powder was introduced between the sheets, and the residual air was evacuated. The atmospheric pressure on both sides of the filter restrains the powder from shifting. The filter is connected to a vacuum reservoir which reduces vacuum loss due to outgassing of the ^{10}B. Radiographic measurements indicated that deviations from uniformity over the 7.0-in. (17.78-cm) diameter of the filter were less than ±4%.

This filter effectively removes neutrons with energies below 4 eV and allows repetition rates of 120 pulses/second with most capture samples. Materials such as gold with a very strong low-energy resonance require a somewhat lower rate, ~ 90 pulses/second.

The low energy portion of the neutron spectrum $\varphi(t)$ can be described by an expression of the form:

$$\varphi(t) = kE_n^a \exp(-\beta/\sqrt{E_n})$$

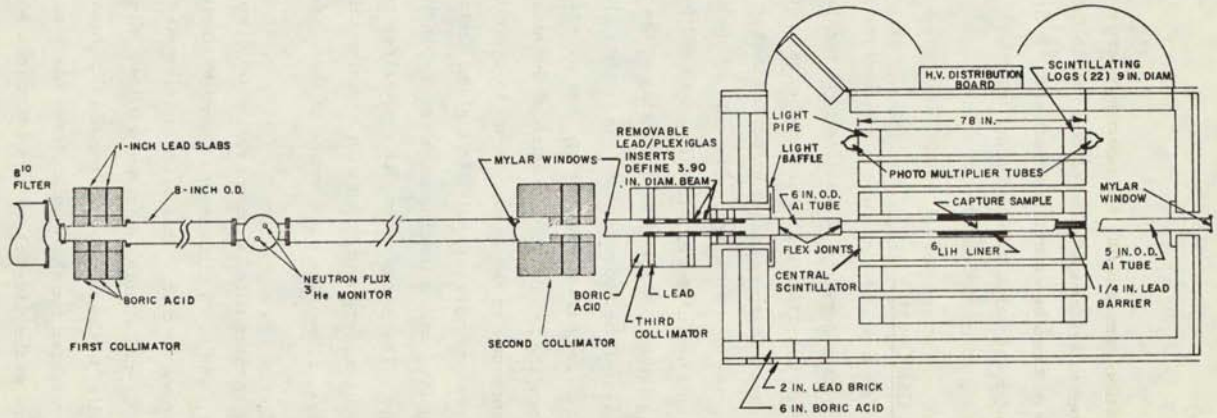

Fig. 3. Facility for capture cross-section measurements located at the end of the 230-meter evacuated neutron flight path

where k is a normalization constant, E_n the neutron energy, and α and β are parameters adjusted to achieve a least-squares fit to the measured flux shape. The value of β can be calculated from the ^{10}B filter thickness and agreed very well with the value obtained from the fit.

2.3 DETECTORS

2.3.1 Proton Recoil Gas Counter

The total cross section of hydrogen has been extensively studied experimentally and is well understood theoretically in terms of effective-range theory. Estimated uncertainties in the total cross section are $< 1\%$, and its freedom from sharp resonant structure makes it an almost ideal cross section for use as a standard. The only open channel besides elastic scattering is radiative capture, which is $\approx$ 330 millibarns at thermal and is entirely negligible compared to scattering at the energies of interest here. The mass of the hydrogen nucleus is very close to that of the neutron, so that a large fractional energy loss occurs in the scattering events. Since the angular distribution of the elastic scattering at these energies is isotroptic in the center-of-mass system, the energy distribution of recoil protons corresponding to a given neutron energy is very nearly rectangular, with a leading edge corresponding to the incident neutron energy. The use of essentially noiseless gas amplification in a proportional counter, combined with commercially available low-noise preamplifiers, allows the observation of these recoil events down to 1 keV or less.

A proportional counter filled with approximately two atmospheres of 94.1% methane (CH_4) and 5.9% nitrogen was used to implement the hydrogen scattering cross section. This 5.08-cm-diameter counter was constructed with a 0.203-cm alumina entrance window. Since the counter axis was parallel to the neutron beam, the flux measurement could be accurately corrected for the window transmission. The maximum correction occurs at the 434-keV oxygen resonance where it

approaches 22 ± 2%. Since the effective active length of an identical xenon-filled counter has been experimentally determined,[1] the absolute efficiency can be accurately calculated. This efficiency is 15.4 ± 0.5% at 100 keV which yields high counting rates at our 230-meter facility. The 0.66-μsec time jitter yields a 9% energy resolution at 100 keV, which is more than adequate for these measurements.

2.3.2 ^{3}He Gas Proportional Counters

Neutron detection with the ^{3}He(n, p)T reaction was implemented with two 1-in. (2.54-cm) diameter cylindrical gas proportional counters containing ^{3}He as the major part (97%) of the filling gas. The active length of the counters is 6 inches (15.24 cm) and the gas pressure is 10 atmospheres. For the flux measurements at the 230-meter facility concurrent with the capture measurements, two counters are located across the outer edges of the 6-in. (15.24-cm) diameter neutron beam (see Fig. 3). The capture measurements utilize the inner 9.91-cm diameter portion of the neutron beam which is not intercepted by the ^{3}He counters.

These ^{3}He counters have been calibrated[1] against $^{10}BF_3$ proportional counters, and hence the response can be directly related to the ^{10}B(n, α)^{6}Li cross section. The calibration was performed with an electronic bias corresponding to 80% of the 764-keV energy released in the ^{3}He(n, p)T interaction with thermal neutrons, and hence this bias was used in the flux measurements reported here.

2.3.3 Large Liquid Scintillator

In order to improve the precision for measurements of materials with low capture cross sections or with a low neutron binding energy, the 600-liter scintillator in use at the beginning of the contractual period was replaced with a 2400-liter scintillator. This larger detector yields a much improved signal-to-background ratio due to its better summing characteristics for capture gamma cascades. In effect, this means that

the average energy deposition per capture event is increased, and the fraction of the capture events above a given bias is therefore much larger. The good gamma-ray energy resolution of the smaller detector was preserved with a modular form of construction.

The 2400-liter detector consists of the container used for the old 600-liter detector surrounded by a closely packed array of 22 nine-inch (22.86-cm) diameter by 78-inch (198.12-cm) long cylindrical scintillators. These cylindrical scintillators (logs) are similar to those used in a 4000-liter scintillator[16] located at the 20-meter flight path facility. Measurements of capture pulse-height distributions for gold using the 4000-liter detector, which contains 44 logs, indicated that the addition of 22 logs to the central tank would yield good capture gamma cascade summing and a relatively low ambient background rate.

Since capture gamma cascades usually possess a relatively high multiplicity, it is possible to discriminate against single gamma-ray background events by using coincidence techniques. For this reason the central 24-in. (60.96-cm) diameter central scintillator is optically split in the vertical plane parallel to the neutron beam. The photomultiplier anode signals from each of these scintillator halves are summed with the anode signals from the eleven logs on the same side of the scintillator, thus splitting the scintillator into two optically and electronically isolated halves. As will be described later in Section 3.3, each half of the scintillator is provided with its own amplifier-discriminator system which allows the detection of capture gamma coincidences. This same technique has been successfully applied to the 4000-liter detector at the 20-meter flight path for measurements to 20-keV neutron energy.

In the 2400-liter detector, additional isolation between the two halves was obtained by placing a 0.25-in. (0.635-cm) lead sheet between them. The lead intercepts most of the Compton-scattered gamma rays which might produce a coincidence resulting from only a single gamma

ray. Operational experience indicates that in the coincidence mode the signal-to-background ratio is improved by a factor of ten at a sacrifice of a factor of three in net counting rate.

Additional suppression of backgrounds due to sample-scattered neutrons was achieved by surrounding the capture sample with a sleeve of ^{6}LiH, 1.64-cm thick and 61-cm long. This sleeve moderates and captures neutrons in the ^{6}Li(n, α)T reaction and thus appreciably reduces the fraction of the neutrons which can moderate in the scintillator and produce 2.2-MeV capture gamma rays via the H(n, γ)D reaction. The background due to ambient gamma rays and LINAC-associated neutrons has been significantly reduced by surrounding the scintillator with a 2-in (5.08-cm) thick layer of lead and a 6-in. (15.24-cm) layer of boric-acid shielding. A double thickness of shielding was placed on the side facing the LINAC.

Small-angle scattering from the inside surface of the last collimator can contribute to the time-dependent background, and for this reason the last collimator is composed of alternate lead and plastic rings machined with a 2° taper on the inside surface. This effectively prevents the inside surface from being directly illuminated by gamma rays or neutrons from the LINAC neutron source.

A photograph of the scintillator taken during its construction is shown in Fig. 4.

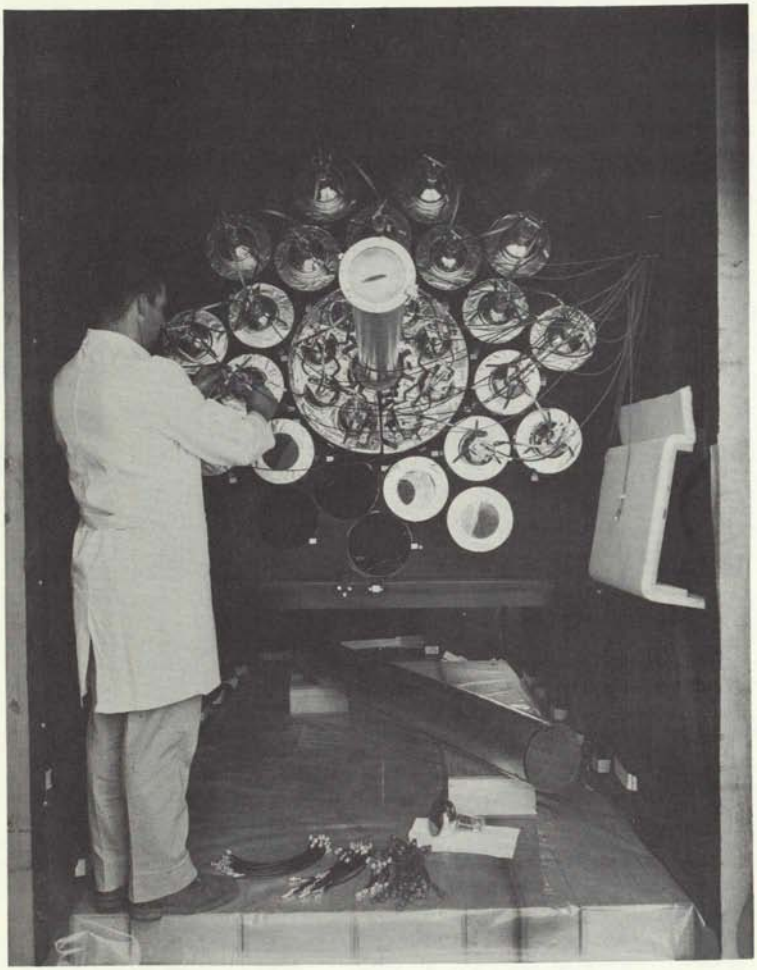

Fig. 4. Photograph of the 2400-liter scintillator under construction

3. DATA ACQUISITION TECHNIQUES

A CDC-1700 computer serves as the central element in our "on-line" data acquisition system. Some of the features of this computer are:

1. A 1.1-μsec central processor with 16,000 words of 16-bit memory.

2. A two-parameter TMC interface bin, capable of accepting most of the pulse height and timing modules available.

3. An interface to the Eldorado 5-nsec time interval device.

4. An IBM compatible seven-track, 556-bit/inch magnetic tape drive.

5. A 1.5×10^6 word magnetic disk drive unit with 15 changeable disk packs.

6. Fourteen interrupt data lines.

7. A digital-to-analog interface used to drive an oscilloscope.

8. A punched card reader.

9. A plotter.

10. A very fast Hewlett-Packard ADC with digitizing rate of 200 MHz.

11. A general-purpose interface bin which allows the addition of new devices to be made simply and cheaply. This bin has so far been used to interface the plotter, card reader, and Hewlitt-Packard ADC.

The capabilities for high-speed data acquisition, coupled with the large storage area of the magnetic disk, allow simultaneous storage of two time-of-flight spectra, or of pulse height vs. time-of-flight data.

3.1 FLUX ABOVE 80 keV

For the measurement of the neutron flux from 80 keV to 1 MeV with the methane-filled proton-recoil proportional counter described in Section 2.3.1, a two-parameter mode of data acquisition was used in which the neutron flight time and proton-recoil pulse amplitude were stored as pairs of binary numbers. Typically, the time information was stored in 80-nsec increments, and the pulse height was stored in 1024 increments of 1 keV each to span proton-recoil energies of roughly 20 keV to 1 MeV. A precisely determined deadtime of 160 μsec was introduced in the timing signals from the methane counter to avoid ambiguities in the deadtime correction due to the variable deadtime characteristic of the analog-to-digital converter. Since 160 μsec considerably exceeds the sum of the maximum digitizing time plus the computer processing time, the deadtime corrections could be made very precisely. These corrections never exceeded 30% in the present data.

To avoid any mismatch between time and pulse-height information, the same pulse that stopped the time analyzer also opened the gate to the analog-to-digital converter. The linearity and gain stability of the entire system was determined with a precision mercury pulser. Since the methane counter had a small (5.9%) admixture of nitrogen, it was possible to estimate the energy scale of the system before the experiment by observing the 616-keV events from the $^{14}N(n,p)^{14}C$ induced by thermalized neutrons from a PuBe neutron source. The final energy scale is established from the two-parameter data as described in Section 4.1. A block diagram of the electronics used with the methane counter is shown in Fig. 5.

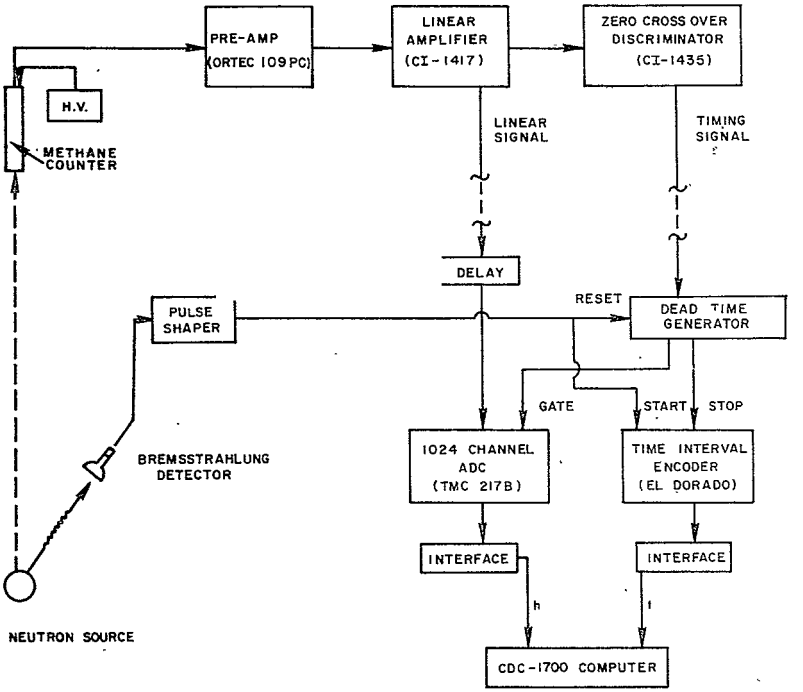

Fig. 5. Simplified block diagram of electronics used with methane gas proportional counter

3.2 FLUX BELOW 80 keV

By making use of one of the two time-of-flight data channels in the computer, the flux spectrum was continuously monitored during the capture measurements with the ^{3}He proportional counters. The ^{3}He signals were off-gated for ≈10 μsec to avoid effects from the gamma flash and fed to a scaler to serve as a neutron intensity monitor. The ^{3}He signals were also on-gated to a second scaler in the 7,500- to 8,000-μsec period after the LINAC burst to obtain the background counting rate. This background due to low energy neutrons from cosmic rays and the LINAC was typically 2 to 4% of the foreground signal. Further details of the flux measurements are given in last year's annual report.

3.3 CAPTURE DATA

The gamma-ray energy scale of the scintillator was established using ^{142}Pr and ^{24}Na sources. Two bias windows were then established: 3.5 to 10 MeV and 4.5 to 10 MeV. A third bias condition was established by requiring that the 3.5- to 10-MeV events correspond in time to a coincidence of events depositing more than 1 MeV in each half. The coincidence resolving time was 80 nsec. These coincidence data, along with the two noncoincidence data channels, were delayed in passive 50-μsec delay lines to allow the time analyzers to accumulate time-of-flight data immediately prior to the linac burst. These pre-burst data provided valuable checks on the ambient background in each data channel. The ambient background was also measured after each data run with the LINAC off. The agreement between the two types of ambient determination was excellent except for ^{238}U, where a small amount of short-lived induced activity was detected.

The coincidence data were accumulated in one of the computer time-of-flight channels, and the two noncoincidence data channels were accumulated on two (TMC-211) 1024-channel time analyzers. The consistency of the capture data taken under these three bias conditions is

a very sensitive check for background subtraction errors or unexpected changes in capture gamma-ray detection efficiency with incident neutron energy. The block diagram of the electronics used for capture data acquisition is shown in Fig. 6.

The samples used in the capture measurements were high-purity metal disks of natural isotopic composition except for U which consisted of 99.8% ^{238}U. The samples were approximately 11 cm in diameter and had the following thicknesses in units of 10^{-3} atom/barns: 17.58 (Mo), 7.15 (Ta), and 5.55 (^{238}U).

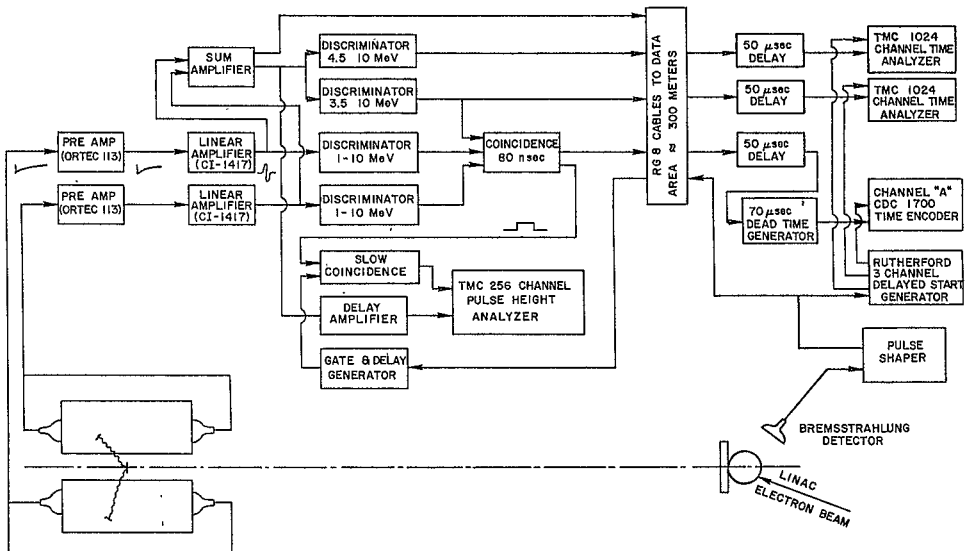

Fig. 6. Block diagram of electronics used for capture data acquisition

4. DATA ANALYSIS

FLUX SHAPE

The first step in obtaining the neutron spectrum was the comparison of the ^{3}He time-of-flight data sets taken during the successive capture measurements in order to conform that the spectrum did not change during the running period. Since the spectrum depends primarily upon the geometrical configuration of the LINAC target and moderator, it can be expected to be very stable and reproducible. This was confirmed by the experimental comparisons, after which the ^{3}He spectrum runs were summed to improve the statistical precision. The summed data were then divided by the previously measured ratio of ^{3}He to BF_3 response functions to obtain a spectrum related to the $^{10}B(n, \alpha)^{7}Li$ cross section below 80 keV.

One set of two-parameter proton-recoil data comprising $\approx 7 \times 10^5$ events was taken for each running period. These two-parameter data were sorted by the CDC-1700 on-line computer into pulse-height distributions corresponding to $10\% \frac{\Delta E}{E}$ neutron-energy bins for the purpose of determining the energy scale of the system.

The background pulse-height distribution was obtained by sorting the data corresponding to very long flight times (i.e., very low neutron energies) so that the proton recoil energies are less than the discrimination level. This long flight time data represents the only source of background since an earlier experiment indicated that extraneous proton recoils from scattered neutrons were negligible.

After the recoil distributions are corrected for deadtime and background, the leading edges of the semi-rectangular distributions are taken be be proportional to the pulse height corresponding to the mean

neutron energy. This leading edge parameter was found to be linearly related (within ~2%) to the neutron energy after correction for the zero offset of the analog-to-digital converter.

Using the linear relationship thus obtained, the two-parameter data were corrected for deadtime and sorted into 80 nsec channel width time-of-flight information biased at a pulse height corresponding to 30% of the neutron kinetic energy to eliminate carbon and nitrogen recoil events. This time-of-flight information was then corrected for the attenuation of the alumina end window of the methane counter, wall effects, multiple scattering, background and the self-shielding effect. The corrected data, when divided by the hydrogen cross section, yielded the flux shape above 80 keV.

The ^{3}He and n+p flux shapes were normalized in the energy region 80-100 keV to obtain a composite flux shape extending over the entire energy range of these measurements. This composite flux shape normalized to the linac power level is shown in Fig. 7. The units in the figure are neutrons/amp μsec^{2}/cm^{2} vs. neutron energy, i.e., the number of neutrons/cm^{2} observed in a 1-μsec time channel corresponding to neutron energy E when the LINAC is operated with a 45-MeV electron energy, 1 amp of beam current and a burst width of 1 μsec.

4.2 CAPTURE DATA

The time histories recorded from the scintillator with the various capture samples in place were corrected for deadtime effects (<4%), and three backgrounds were subtracted:

1. Ambient background. The counting rate observed in the 50-μsec immediately preceding the LINAC burst was taken to be the ambient background. This ambient background correction was checked in the regions between low-energy resonances. This background was also checked by observing the counting rate with the LINAC off, as discussed previously.

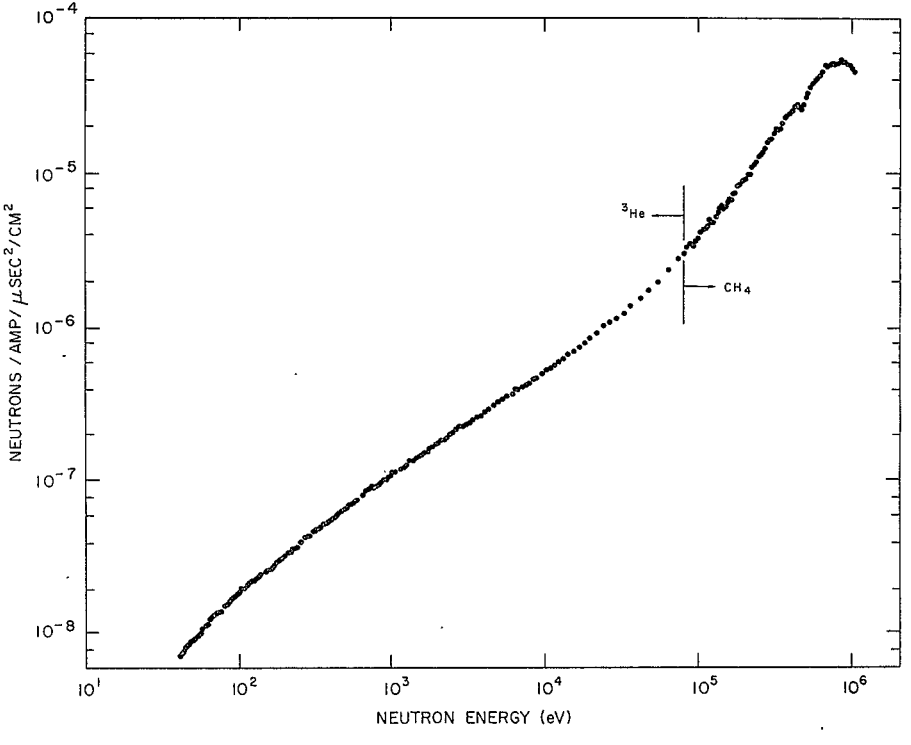

Fig. 7. Composite flux shape normalized to LINAC beam parameters (electron energy ≈ 45 MeV)

2. Sample out background. The counting rate observed with no sample in the beam is due to extraneous neutrons from the LINAC and was very small in all cases because of the well-collimated beam employed. The time dependence of this correction is similar to that of the neutron flux.

3. Scattered-neutron background. As mentioned earlier, the use of the ^{6}LiH liner reduces the effect of sample-scattered neutrons significantly. To obtain a measure of the remaining scattered-neutron background, measurements were performed using 0.635-cm-thick samples of high-purity carbon or lead. The capture signals observed with either of these materials in place can be assumed to be proportional to the detection of inscattered neutrons, since the capture cross sections of these materials are negligible.* The ratio of the scattering probabilities of the capture sample and the Pb or C samples was evaluated at a neutron energy that takes into account the slowing-down time of neutrons in the scintillator. Since the energy loss suffered by the inscattered neutrons is quite different for these two materials, the difference between the inscattering corrections, after normalization to the respective scattering probabilities, for C and Pb is a measure of the energy loss effect combined with the effective scattering cross-section uncertainties. The discrepancy was $\approx$20%, and this figure was taken to be a measure of the scattering-background uncertainty.

After all of the backgrounds are subtracted, the observed noncoincidence capture time histories are corrected for the change in the scintillator pulse-height spectrum fraction due to the increase in the compound-nucleus excitation energy. This correction was obtained using capture pulse-height distributions taken in the 110 to 400 eV neutron energy region. These pulse height distributions were taken to be appropriate to capture at zero neutron energy since these neutron energies are negligible compared to the neutron separation energies of the

*An exception to this occurs at the low energy lead resonances which produce an observable capture rate.

compound nuclei. The assumption is also made that the effect of the neutron kinetic energy is to stretch the zero-energy pulse height distribution in a linear fashion. Thus, we first calculate an effective bias:

$$\Sigma' = \Sigma \left(\frac{E_B}{E_B + E_n} \right), \tag{2}$$

where Σ is the gamma energy bias (3.5 or 4.5 MeV), E_B is the neutron separation energy of the compound nucleus and E_n is the kinetic energy of the neutron captured. The capture cross section correction factor $C_N(E_n)$ is obtained from the relation

$$C_N(E_n) = \frac{\int_{\Sigma'}^{\infty} P(\Sigma) d\Sigma}{\int_{\Sigma}^{\infty} P(\Sigma) d\Sigma}, \tag{3}$$

where $P(\Sigma)$ is the number of gamma events observed in the interval $d\Sigma$. The capture pulse-height distributions for molybdenum is illustrated in Fig. 8.

In the case of coincidence data an additional correction $C_C(E_n)$ multiplies the above $C_N(E_n)$. Since the probability of observing a coincidence is proportional to the product of the probabilities of detecting the capture event in either half of the scintillator, the effect of the neutron kinetic energy is treated as $C_C(E_n) = C_A(E_n)\ C_B(E_n)$ where $C_C(E_n)$ is the coincidence cross section correction and $C_A(E_n)$, $C_B(E_n)$ are the correction factors for the A and B halves of the scintillator as a function of neutron energy. Since the two halves of the scintillator are essentially identical, we can take $C_A(E_n) \approx C_B(E_n) \approx C(E_n)$, thus $C_C(E_n) \approx C^2(E_n)$, where the quantity $C(E_n)$ is obtained as in Eqs. (2) and (3) with the important exception that the pulse height distribution as observed in one half of the scintillator must be used to obtain the correction. Since it

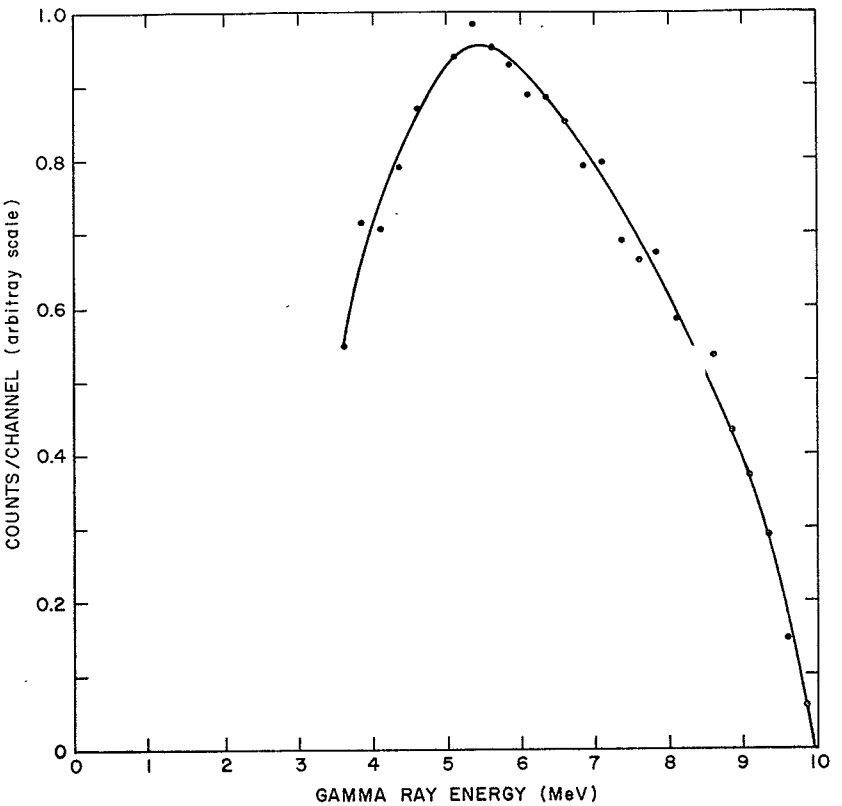

Fig. 8. Pulse-height distribution from 2400-liter scintillator resulting from capture in low energy molybdenum resonances

was not practical to measure this pulse height distribution directly, it was estimated using distributions measured with a ^{24}Na source. The uncertainty in this estimate represents the major uncertainty in the coincidence data correction. Due to this uncertainty, the noncoincidence data were used where $C_C(E_n)$ differed appreciably from unity.

After the above corrections were performed, the three capture time histories (3.5- and 4.5-MeV bias noncoincidence plus 3.5-MeV bias coincidence) for each sample were compared for consistency. The agreement was excellent in all cases, except for the coincidence data at neutron energies > 200 keV, which is probably due to the approximations employed in the coincidence corrections discussed above.

As an additional check on the reliability of the capture data, an experimental check was performed to obtain a measure of time-dependent gain changes in the three capture data channels using a ^{24}Na source. ^{24}Na decays by the emission of coincident 1.37- and 2.75-MeV gamma rays which produce a 4.12-MeV sum signal in the scintillator peaking near the two capture bias energies. To observe the time-dependent gain shift, a capture sample is placed in the neutron beam; and a ^{24}Na source is placed nearby, but out of the neutron beam. When data taken with the source removed are subtracted from the ^{24}Na data, the difference is the observed "time dependence" of the ^{24}Na counts. Thus, any departure of the ^{24}Na counts from a constant rate is a sensitive measure of efficiency changes in the three capture channels, and this information can be used to ascertain the earliest time after the bremsstrahlung burst at which the scintillator data can be considered to be reliable. For the data reported here, the capture data appeared to be free of bremsstrahlung effects at times corresponding to energies < 3 MeV. The capture yield and backgrounds are illustrated in Fig. 9 for molybdenum.

Having thus obtained corrected capture time histories, the data were corrected for the resonance self-shielding and multiple scattering effects. In the low-keV region, resonance self-shielding and multiple scattering were calculated using the computer code SESH[2] which uses

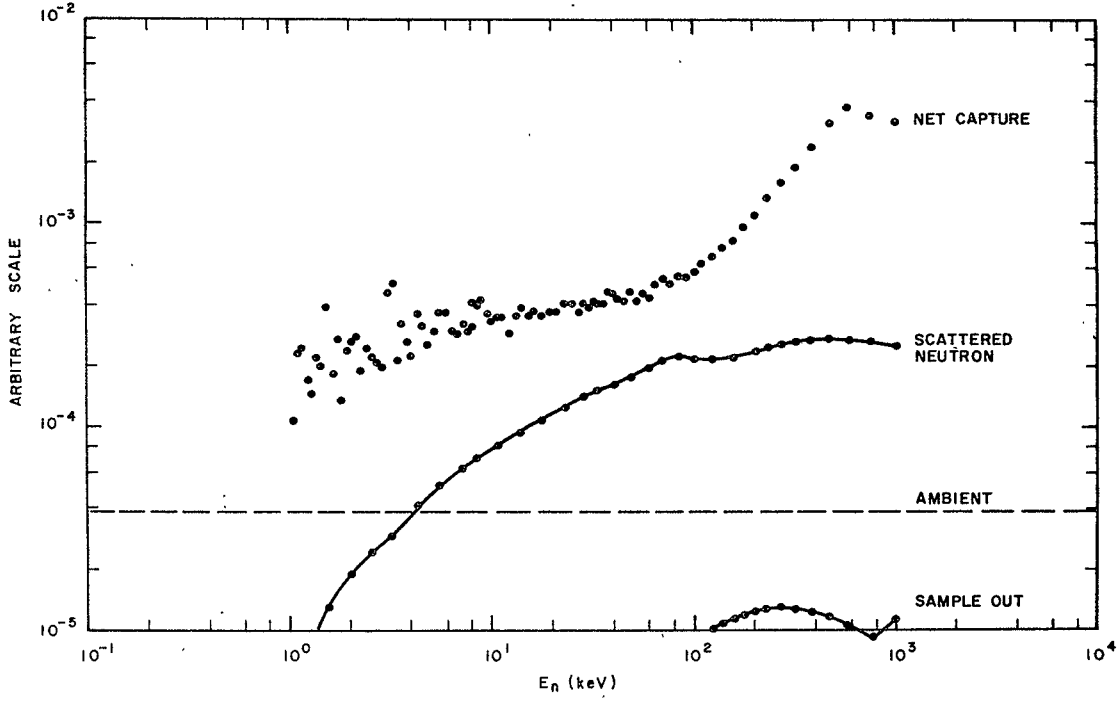

Fig. 9. Capture yields and backgrounds observed during the molybdenum capture cross-section measurements using the 2400-liter scintillator in the noncoincidence mode with 3.5-MeV bias

estimates of the average resonance parameters to generate resonance environments via Monte Carlo techniques. In the high energy region (> 50 keV) resonance self-shielding was negligible, and multiple scattering and self-shielding could be calculated using a smooth cross-section approximation.

The capture yield normalization factors were obtained from measurements of the average capture yield in the 2-8 keV region along with the very low energy resonance region using the 20-meter flight path and the 4000-liter scintillator. For the sample thicknesses used in these measurements, the neutron transmission was essentially zero in the low-energy resonances, i.e. they were "saturated". If the neutron width is small compared to the total width, as is usually the case, the counting rate in the peak region is insensitive to errors in the resonance parameters; and hence the average yield in the 2-8 keV interval can be converted to an average capture probability with a very small uncertainty. This allows the capture yield data obtained with the 230-meter flight path to be converted to a capture cross section by normalization in this same energy interval. The normalization procedure is illustrated in Fig. 5 of Appendix I. An example of the calculated[3] vs. measured shape for a saturated ^{238}U resonance is shown in Fig. 10, and several normalizations obtained from resonances in tantalum are compared to the measured energy dependence of the flux shape in Fig. 11.

An alternate procedure which serves as a check on the above technique is the comparison of capture areas of resolved resonances near the low-energy end of the 230-meter capture data (≈ 70 eV). These areas may be used to normalize the capture yield within the uncertainties associated with the published resonance parameters.

As has been explained previously in detail,[1] normalization of the capture yield measured with the 20-meter flight path is accomplished by determining the product of the absolute flux and the efficiency for detecting capture gamma rays (the quantity $<\epsilon_o SCT_\gamma>$ in the notation of

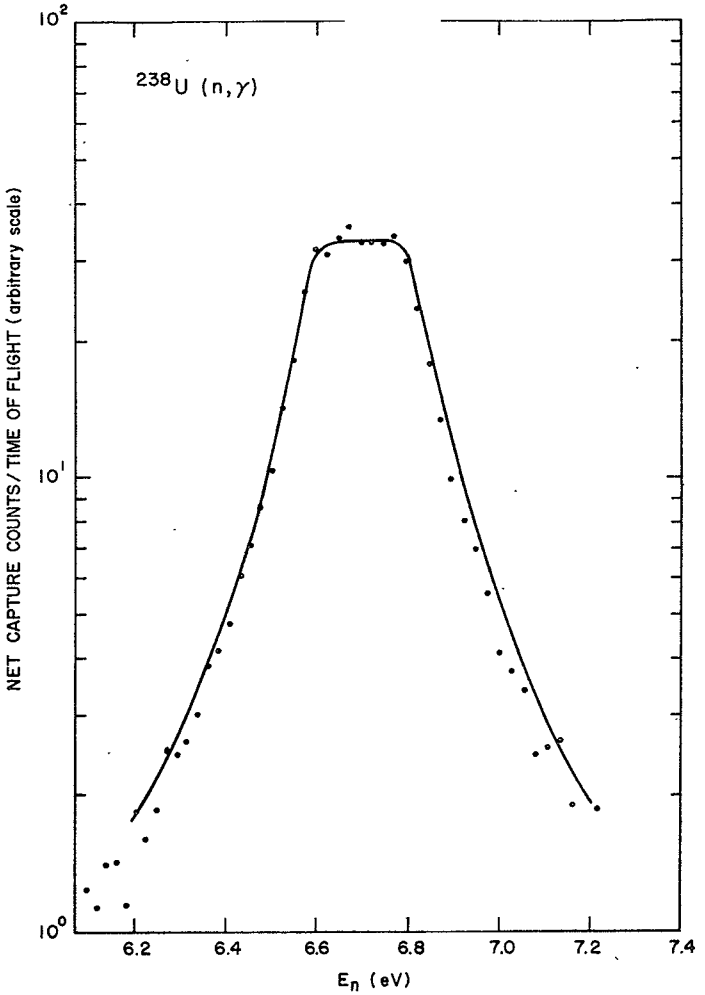

Fig. 10. Comparison of the observed vs calculated yield for the saturated 6.67-eV resonance in ^{238}U

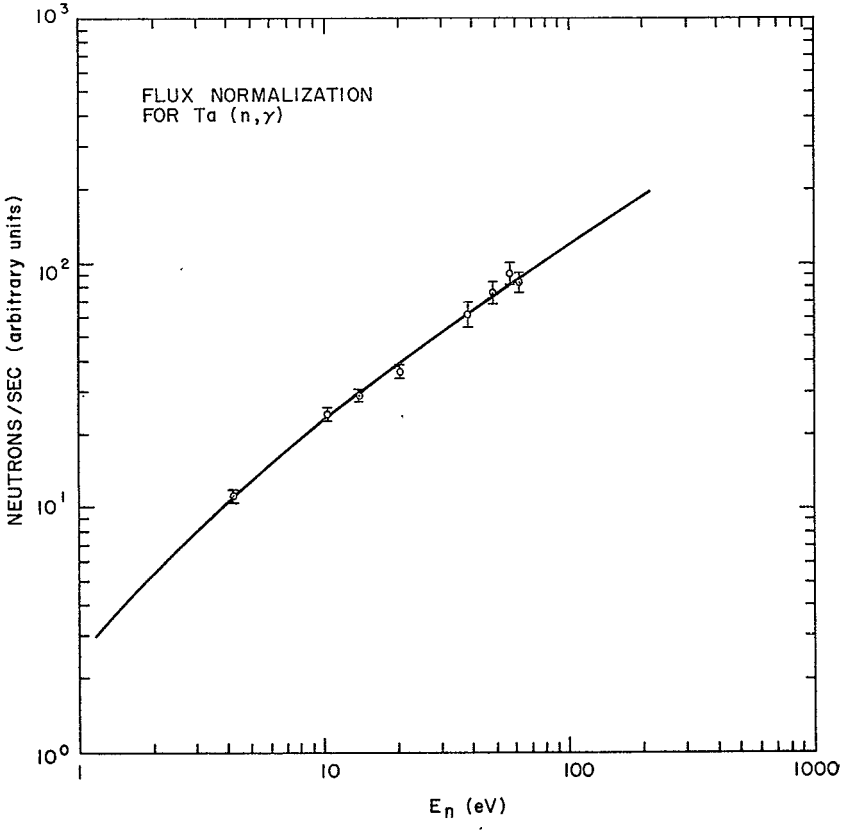

Fig. 11. Flux normalizations obtained for tantalum resonances compared to the measured energy dependence of the neutron flux

Ref. 1). For ^{238}U, this quantity was determined with an uncertainty of ±2% from the calculated capture probability near the peak of the saturated resonance at 6.7 eV. The normalization deduced from this resonance also agreed within 5% with that deduced from the capture areas of the resonances at 36.9 and 66.3 eV which were calculated with the parameters of Ref. 4. Another check on the normalization of ^{238}U was obtained from the resonances at 81 and 117 eV observed in the data obtained with the 230-meter flight path. These areas could be determined to ~± 20% (including uncertainties both in our measurements and the existing[4] resonance parameters), and the normalization deduced from these resonances agreed within 10% with the more accurate value obtained from the 6.7-eV resonance. The normalization of the ^{238}U capture yield is judged to be determined with an accuracy of ±5%.

Normalization of the capture yield for Ta was obtained from the capture areas of eight resonances at 4.28, 10.34, 13.85, 20.34, 39.03, 48.98, 57.4 and 62.95 eV; the first four of which had peak capture probabilities ≥ 0.95 for the sample thickness used. The normalization factors deduced from the saturated resonances could be determined within ±5%, and these four factors agreed within 7%. The normalization factors deduced from the four resonances at higher energies using the parameters of Ref. 5 could be established to ~± 10%, and these factors also agreed with the low-energy results within their uncertainties. The normalization of the Ta yield obtained from these eight resonances is judged to be established within an uncertainty of ±5%.

The normalization of the capture yield for natural Mo was obtained from an average of the normalization factors for the seven isotopes which were weighted by the isotopic abundance and the average capture cross section. The parameters of Refs. 6, 7, 8 were used to calculate the capture areas of observed resonances at 12.08 eV in ^{98}Mo, 44.65 eV in ^{95}Mo, 70.93 eV in ^{97}Mo, 97.5 eV in ^{100}Mo, 131.4 eV in ^{96}Mo and

159.5 eV in ^{95}Mo. Except for the 44.65-eV resonance in ^{95}Mo, which had the largest peak capture probability of 0.68 for the sample used, the shapes of the capture resonances calculated with the existing parameters agreed very poorly with our data. This gave rise to uncertainties in the normalization factors of 10-30% for resonances other than the 45-eV level in ^{95}Mo+n, for which the normalization could be established to about ±5%.

To supplement these data, scintillator pulse-height distributions were measured for the same Mo resonances in order to deduce their detection efficiencies relative to that of the 45-eV resonance in ^{95}Mo+n by ascertaining their relative pulse-height spectrum fractions above the electronic bias. These spectrum fractions agreed well with that calculated from the spectrum observed for the ^{95}Mo resonance assuming this distribution also applies to the other isotopes but is stretched linearly with the neutron binding energy. Consequently, such a calculation was used to estimate the efficiencies for ^{92}Mo and ^{94}Mo, where satisfactory resonance capture areas or pulse-height distributions were not obtained experimentally.

An additional difficulty arises in calculating the average yield normalization factor for the natural Mo sample, since the average isotopic capture cross sections are not well established. Statistical-model calculations of these cross sections were made from available resonance-parameter data, and in some cases s-wave level spacings were estimated from the Fermi-gas model including shell and pairing corrections. The normalization for natural Mo, including both the uncertainties in the isotopic efficiencies and that introduced by the absence of isotopic cross-section information, is judged to be determined to within ±20%. This uncertainty cannot be reduced further without individual measurements of the capture cross sections for at least three of the separated isotopes (^{95}Mo, ^{97}Mo and ^{98}Mo) that contribute most of the capture cross section for the natural material.

5. RESULTS

The average capture cross sections for Ta, Mo and ^{238}U are given in Tables 1-3 and are illustrated in Figs. 12, 13, 14. Also listed are relative uncertainties calculated from a quadrature sum of five components:

1. Statistical uncertainties in the net capture yield, including contributions from the three backgrounds (ambient, scattered-neutron, and sample-out).

2. Statistical uncertainties in the neutron flux data.

3. Statistical uncertainties in the Monte Carlo calculations of multiple-scattering and self-shielding effects that arise from a finite number of neutron histories.

4. An estimated 20% uncertainty in the correction applied at high energies for the capture γ-ray spectrum-fraction change due to the variation of incident neutron kinetic energy.

5. An estimated 20% uncertainty in the calculated resonance self-shielding effect. This effect is defined as the difference between finite-sample corrections calculated with the methods of Ref. 2 and those calculated with a smooth cross-section approximation.

In addition to the relative uncertainties listed in Tables 1-3, systematic uncertainties have been evaluated which primarily affect the normalization (and not the shape) of the capture excitation function. These were taken to be a quadrature sum of the uncertainty in the capture-yield normalization factor, the uncertainty in the yield near 10 keV due to a 20% uncertainty in background subtractions, and a 5% uncertainty in the flux data due to possible deviations of the $^{10}B(n, \alpha)$ cross section from (1/v)

Table 1

NEUTRON CAPTURE CROSS SECTION FOR NATURAL TANTALUM

Energy (keV)	Cross Section (barn)	Relative Uncertainty (percent)
.9576	12.6	12
1.009	8.52	11
1.064	9.92	11
1.124	7.65	10
1.190	8.70	10
1.253	8.03	10
1.321	8.91	10
1.393	6.99	10
1.469	4.79	10
1.553	6.30	10
1.645	6.93	9
1.745	6.43	9
1.843	5.17	9
1.941	4.40	9
2.046	5.58	9
2.161	5.68	9
2.285	5.38	9
2.420	4.61	9
2.568	4.96	9
2.730	4.06	9
2.890	3.55	9
3.044	3.86	9
3.209	3.54	9
3.393	3.53	9
3.588	3.46	9
3.800	3.45	9
4.036	2.90	9
4.290	3.40	9
4.569	2.53	9
4.877	2.82	9
5.171	2.16	9
5.451	2.62	8
5.748	2.77	8
6.070	2.52	8
6.420	2.30	8
6.807	2.12	8
7.226	2.10	8

Table 1 (Continued)

Energy (keV)	Cross Section (barn)	Relative Uncerta (percent)
7.690	2.17	8
8.191	1.98	8
8.743	1.89	8
9.362	1.74	8
10.04	1.73	8
10.80	1.69	8
11.50	1.66	8
12.12	1.57	8
12.77	1.54	8
13.48	1.51	8
14.26	1.27	8
15.10	1.20	8
16.02	1.31	8
17.03	1.23	8
18.14	1.26	8
19.35	1.14	8
20.70	1.11	8
22.19	1.11	8
23.86	1.10	8
25.70	.988	8
27.77	.943	8
30.12	.876	8
32.78	.811	8
35.78	.800	8
39.23	.743	8
43.19	.720	8
46.57	.625	8
49.01	.706	8
51.72	.596	8
54.64	.601	8
57.82	.646	7
61.22	.594	7
64.99	.614	7
69.12	.502	7
73.65	.512	7
78.63	.527	7
84.22	.539	7

Table 1 (Continued)

Energy (keV)	Cross Section (barn)	Relative Uncertainty (percent
90.32	.437	7
97.10	.484	7
104.7	.472	7
113.3	.450	7
123.0	.423	7
133.8	.389	7
146.3	.340	6
160.6	.328	6
176.9	.317	6
196.1	.310	6
218.5	.296	5
245.1	.290	5
276.5	.258	5
314.7	.252	5
361.4	.220	5
418.8	.205	5
491.7	.201	4
585.2	.174	4
708.5	.163	5
835.5	.142	4
1107.5	.124	9

Table 2

NEUTRON CAPTURE CROSS SECTION FOR NATURAL MOLYBDENUM

Energy (keV)	Cross Section (barn)	Relative Uncertainty (percent)
.9576	.233	21
1.009	.539	21
1.064	.541	21
1.124	.600	21
1.190	.534	21
1.253	.515	20
1.321	.338	20
1.393	.574	19
1.469	.417	19
1.553	.850	18
1.645	.327	18
1.745	.694	17
1.843	.335	17
1.941	.536	16
2.046	.476	16
2.161	.694	16
2.285	.421	16
2.420	.567	16
2.568	.456	15
2.730	.327	15
2.890	.274	15
3.044	.410	15
3.209	.826	15
3.393	.382	15
3.588	.352	15
3.800	.454	15
4.036	.279	14
4.290	.442	14
4.569	.410	14
4.877	.449	14
5.171	.259	14
5.451	.408	13
5.748	.386	13
6.070	.472	13
6.420	.296	13
6.807	.348	13
7.226	.322	13

Table 2 (Continued)

Energy (keV)	Cross Section (barn)	Relative Uncertainty (percent)
7.690	.302	13
8.191	.264	13
8.743	.340	12
9.362	.257	12
10.04	.289	12
10.80	.267	13
11.50	.222	13
12.12	.233	14
12.77	.193	14
13.48	.190	15
14.26	.195	15
15.10	.194	15
16.02	.188	14
17.03	.165	14
18.14	.199	14
19.35	.172	14
20.70	.154	13
22.19	.138	13
23.86	.132	13
25.70	.145	12
27.77	.137	12
30.12	.129	13
32.78	.126	13
35.78	.111	13
39.23	.106	13
43.19	.099	14
46.57	.0940	14
49.01	.0921	14
51.72	.0825	14
54.64	.0840	14
57.82	.0835	14
61.22	.0829	14
64.99	.0753	14
69.12	.0740	14
73.65	.0687	14
78.63	.0616	14
84.22	.0690	14

Table 2 (Continued)

Energy (keV)	Cross Section (barn)	Relative Uncertainty (percent)
90.32	.0692	13
97.10	.0628	13
104.7	.0547	12
113.3	.0544	12
123.0	.0543	12
133.8	.0446	12
146.3	.0497	11
160.6	.0446	11
176.9	.0438	11
196.1	.0381	10
218.5	.0375	9
245.1	.0379	8
276.5	.0372	7
314.7	.0374	6
361.4	.0346	6
418.8	.0354	5
491.7	.0356	5
585.2	.0319	4
708.5	.0311	4
835.5	.0265	4
1107.5	.0215	9

Table 3

NEUTRON CAPTURE CROSS SECTION FOR ^{238}U

Energy (keV)	Cross Section (barn)	Relative Uncertainty (percent)
1.005	1.73	12
1.060	1.79	12
1.120	3.15	12
1.185	3.03	12
1.250	2.37	12
1.316	.960	12
1.387	1.80	12
1.463	1.60	12
1.547	1.27	11
1.637	1.68	11
1.736	2.07	11
1.834	1.19	10
1.931	1.41	10
2.036	1.36	10
2.150	1.61	10
2.274	1.59	10
2.408	1.62	10
2.555	1.31	10
2.716	1.22	9
2.873	1.02	9
3.026	1.03	9
3.190	1.41	8
3.369	1.32	8
3.563	.927	8
3.774	.908	7
4.004	.896	7
4.256	.900	7
4.533	.626	7
4.838	.982	7
5.130	.749	7
5.402	.777	7
5.697	.906	7
6.016	.853	6
6.363	.768	6
6.741	.645	6
7.154	.755	6
7.606	.700	6

Table 3 (Continued)

Energy (keV)	Cross Section (barn)	Relative Uncertaint (percent)
8.102	.642	6
8.648	.627	6
9.251	.676	6
9.920	.735	6
10.66	.643	5
11.35	.614	5
11.95	.639	5
12.59	.581	5
13.29	.622	5
14.05	.599	5
14.88	.562	5
15.78	.542	5
16.76	.570	5
17.85	.523	5
19.03	.527	5
20.35	.543	5
21.80	.548	5
23.42	.505	5
25.22	.482	5
27.23	.464	5
29.50	.464	5
32.07	.455	5
34.98	.450	5
38.31	.433	5
42.14	.401	5
45.39	.392	5
47.77	.339	5
50.36	.356	5
53.15	.359	5
56.19	.308	5
59.49	.298	5
63.10	.295	5
67.04	.288	5
71.37	.255	5
76.12	.252	5
81.37	.230	5
87.18	.224	5

Table 3 (Continued)

Energy (keV)	Cross Section (barn)	Relative Uncertainty (percent)
93.64	.218	5
100.8	.194	5
108.9	.194	5
118.0	.174	5
128.2	.179	5
139.9	.163	5
153.2	.163	5
168.5	.160	5
186.2	.139	5
206.9	.139	4
231.2	.125	4
260.1	.117	4
294.7	.112	5
336.8	.114	4
388.5	.104	4
453.2	.115	4
535.4	.109	5
642.3	.106	6
752.0	.115	10

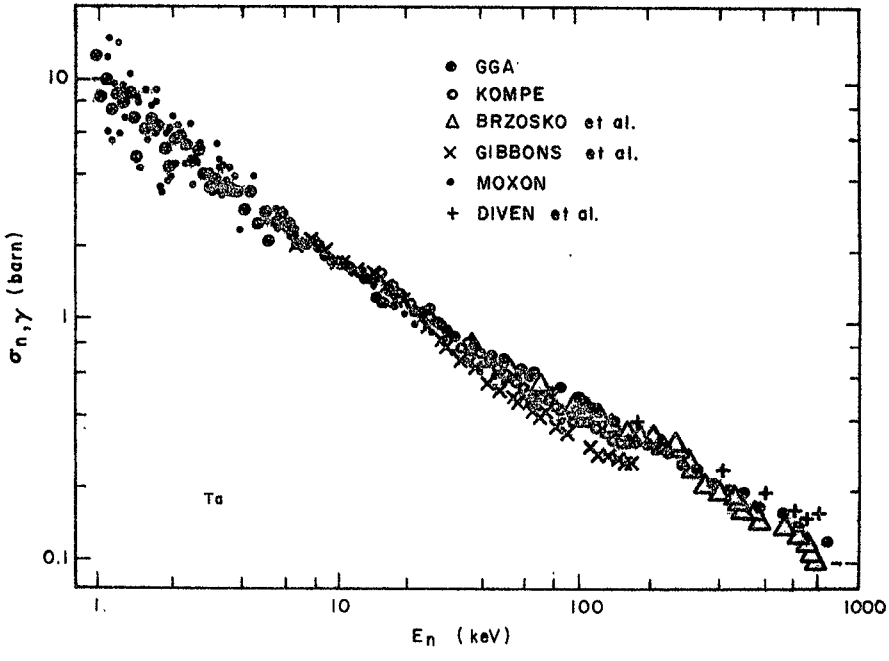

Fig. 12. Capture cross section for tantalum from 1 keV to 1100 keV

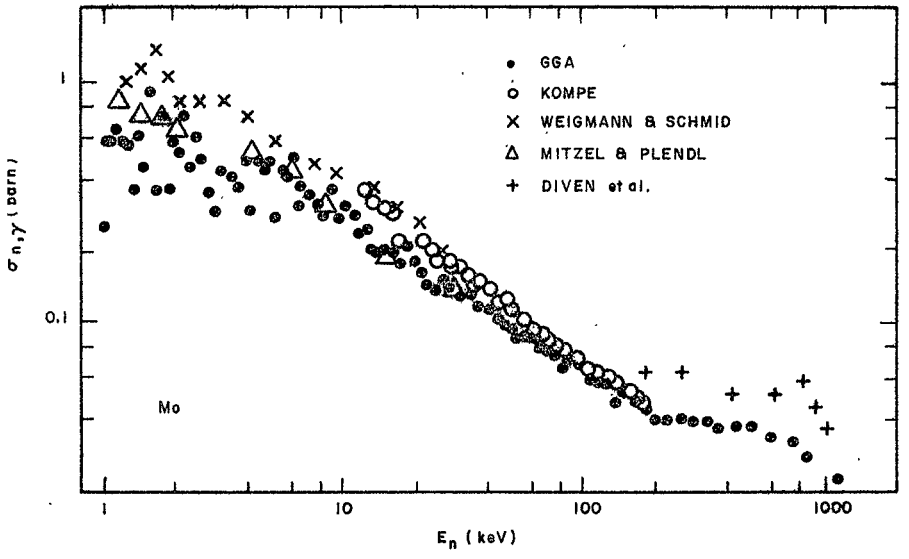

Fig. 13. Capture cross section for molybdenum from 1 keV to 1100 keV

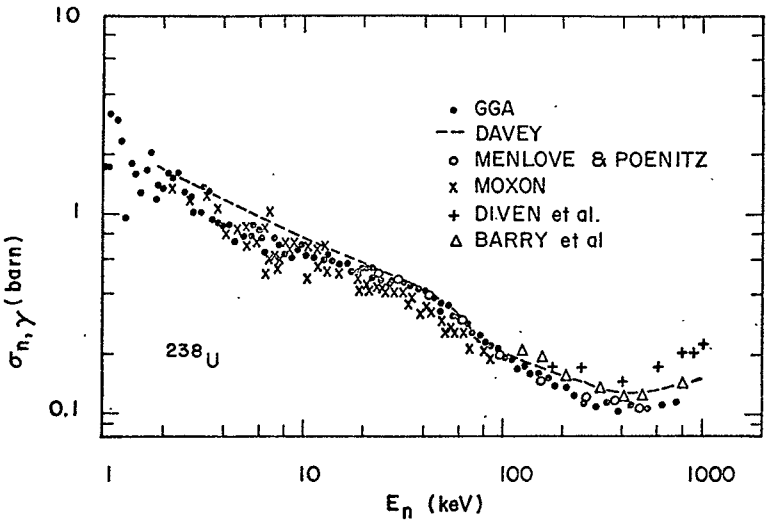

Fig. 14. Capture cross section for ^{238}U from 1 keV to 750 keV

at energies below 80 keV. The total systematic uncertainty thus defined is ±12% for ^{238}U, ±10% for Ta and ±29% for natural Mo.

The capture cross sections for ^{238}U have been corrected for contributions from fission in ^{238}U and in the 0.2% of ^{235}U present in the sample. The ratio of detection efficiencies for fission and capture in our experiment was determined to be approximately unity from previous measurements at this laboratory of capture and fission in ^{236}U and ^{239}Pu. The correction to the ^{238}U capture data is 5% at 750 keV, 2% near 500 keV, 1.5% near 100 keV, and <1% at and below 10 keV.

6. CONCLUSIONS

Absolute average capture cross sections have been obtained for ^{238}U, Ta and Mo over the unprecedented neutron energy range 1-1000 keV. The quadrature sum of relative and systematic uncertainties is ~10-15% for ^{238}U and Ta over the full energy region. The relative uncertainties for Mo are of similar magnitude, but the uncertainty in normalization is much larger (20-30%). Previous data for Mo(n, γ) are subject to similar (or larger) systematic uncertainties, so that the present results cannot be arbitrarily adjusted to conform with the results of other experiments. Capture measurements for separated isotopes of Mo are required to reduce these uncertainties, and there are also indications that much of the existing resonance-parameter information is inaccurate for all of the Mo isotopes. The latter observation leads us to remark that multiple-scattering and self-shielding calculations for bulk media which are made with the existing Mo resonance parameters are very likely to be incorrect.

The present data do not rely upon other standard neutron cross sections for normalization, and the shape of the capture excitation functions above 80 keV are based directly on the exceedingly well-known hydrogen scattering cross section. The present results can thus be expected to differ from some of the earlier, more indirect measurements. Our data are compared to previous results in a paper included in the appendix to this report. Major discrepancies are observed between our data and such early (1960-62) measurements as those of Gibbons et al.[9] for Ta and of Diven et al.[10] for ^{238}U. Most of the more recent data for Ta are in good agreement with our results. For ^{238}U, our data agree almost exactly with the measurements of Menlove and

Poenitz[11] and disagree significantly with the recent data of Moxon[12] and also with the recent evaluation of Davey.[13] For Mo, we are in fair agreement with the results of Mitzel and Plendl[14] at low energies but disagree vastly with the more recent data of Kompe[15] and of Weigmann and Schmid.[7] The Mo excitation function measured by Kompe falls off much more rapidly with energy than does ours, and a similar but smaller discrepancy between our results and Kompe's can be observed for Ta, W and Re (see Appendix A). Kompe's cross sections below 20 keV agree within ~10% with those of Weigmann and Schmid, and our results below 20 keV are ~40% or more lower than these previous data.

We conclude that the present measurements establish the current state of the art in determining absolute average capture cross sections over the full neutron energy region important to the technology of fast-reactor performance and shielding.

REFERENCES

1. W. M. Lopez, et al., Gulf General Atomic Report NASA CR 72474 (1968).

2. F. H. Fröhner, Gulf General Atomic Report GA-8380, January 1968, (unpublished).

3. F. H. Fröhner, General Atomic Report GA-6906, August 1966, (unpublished).

4. J. R. Stehn, et al., Brookhaven National Laboratory Report BNL-325, Second Ed., Supplement No. 2, Vol. III, Z = 88-98 (1965).

5. M. D. Goldberg, et al., Brookhaven National Laboratory Report BNL-325, Second Ed., Supplement No. 2, Vol. IIC, Z = 61-87 (1966).

6. M. D. Goldberg, et al., Brookhaven National Laboratory Report BNL-325, Second Ed., Supplement No. 2, Vol. IIB, Z = 41-60 (1966).

7. H. Weigmann and H. Schmid, Nucl. Phys. A104, 513 (1967).

8. Hla Shwe and R. E. Cote, Phys. Rev. 179, 1148 (1969).

9. J. H. Gibbons, et al., Phys. Rev. 122, 182 (1961).

10. B. C. Diven, et al., Phys. Rev. 120, 556 (1960).

11. H. O. Menlove and W. P. Poenitz, Nucl. Sci. and Engr. 33, 24 (1968).

12. M. C. Moxon, "The Measurement of Average Neutron Capture Cross Sections in the Mass Region Above 100," thesis-London University, July 1968, HL68/3739.

13. W. G. Davey, Nucl. Sci. and Engr. 39, 337 (1970).

14. V. F. Mitzel and H. S. Plendl, Nukleonik 6, 371 (1964).

15. D. Kompe, Nucl. Phys. A133, 513 (1969).

16. E. Haddad, et al., Nuclear Instr. and Methods 31, 125 (1964).

APPENDIX

The following pages contain the texts of two papers describing the GGA capture cross-section program, which have been accepted for presentation at the IAEA Second International Conference on Nuclear Data for Reactors, Helsinki, Finland, June 15-19, 1970.

Measurements of Cross Sections for the Radiative Capture of 1-keV to 1-MeV Neutrons by Mo, Rh, Gd, Ta, W, Re, Au and ^{238}U*

M. P. Fricke, W. M. Lopez,+ S. J. Friesenhahn
A. D. Carlson and D. G. Costello

Gulf General Atomic Incorporated
San Diego, California 92112, USA

1. INTRODUCTION

Radiative capture cross sections for neutrons of energy 1-1000 keV are known to be very important in determing the performance and economy of fast-breeder reactor systems. They are also of considerable interest in establishing statistical properties of nuclei at high excitation energies and for calculations of heavy-element nucleosynthesis in studies of nuclear astrophysics.

Measurements of capture cross sections at these energies have been made in a number of different ways, using different types of neutron sources, different methods to detect the capture events and incident neutrons, and different schemes to establish both the normalisation of the cross section and the shape of the excitation function. Previous capture data from any one measurement have spanned only a portion of the neutron energy region 1-1000 keV, and the results of different measurements have been determined relative to several different standard neutron cross sections. When separate data sets have energies in common, discrepancies of 20-50% in the cross-section values are often observed. In the energy region ~100 keV - 1 MeV it is particularly difficult to accurately establish the incident neutron flux relative to a well-known, primary

* Work supported in part by the U. S. Atomic Energy Commission and by the U. S. National Aeronautics and Space Administration.

+ Present address: University of California at San Diego, La Jolla, California 92037, USA.

standard cross section. Capture data for gold in this region that have been based on the ^{235}U fission cross section of Ref. [1] or [2] have tended [3] to be consistently higher than results normalised by other means. The data above 100 keV are also relatively sparce and have been obtained almost exclusively from measurements made with van de Graaff accelerators. These energies are above those covered by lead slowing-down spectrometers, and previous measurements made with electron linear accelerators have been confined to neutron energies below 200 keV.

In the present paper we describe measurements of capture cross sections which have reduced a number of the uncertainties involved in some of the previous data. The present measurements yield absolute average capture cross sections for eight heavy elements at continuous neutron energy intervals over the region ~ 1-1000 keV. The excitation functions are normalised directly to low-energy (eV) resonances, and their shapes above 80 keV are based directly on the well-known hydrogen scattering cross section. A theoretical interpretation of these and other recent data is presented in the following paper (CN-26/44).

2. EXPERIMENT

Time-of-flight measurements were made with short bursts of photoneutrons produced by bombarding a tungsten-alloy target with 45-MeV electrons from the Gulf General Atomic linear accelerator. The electron target is surrounded by a cylinder of uranium or lead to moderate the neutrons by inelastic scattering and also to shield the detection apparatus from bremsstrahlung. The neutrons are slowed further in a 2.5-cm slab of polyethylene, and a ^{10}B filter is used to prevent overlap of very low-energy neutrons produced from different accelerator bursts.

The neutrons traverse an evacuated flight path containing the collimators and anti-scattering baffles illustrated in Fig. 1. The capture sample is located 230 metres from the neutron-producing target at the centre of a large liquid scintillator used to detect the capture gamma rays. During a capture experiment, the incident neutron flux is monitored by sampling the outer edge of the neutron beam with two ^{3}He gas proportional counters located ahead of the final collimators shown in Fig. 1. This portion of the neutron beam is not viewed by the capture sample. Determinations of the neutron flux and capture γ-ray yield are discussed further in this Section.

The samples used for the capture measurements were all high-purity metal disks approximately 11 cm in diameter and ranged in thickness from 0.1 to 0.25 cm. Except for the ^{238}U sample which was composed of depleted uranium (99.8% ^{238}U), the isotopic composition of the samples was that of the naturally occurring element.

2. 1. Neutron flux

The energy distribution of the incident neutron flux is determined by the time history of counts from the ^{3}He gas proportional counters. The ^{3}He counter was a convenient monitor for use during the capture measurements since it has a high detection efficiency and adequate timing resolution over most of the neutron energy region of interest here. The relative efficiency of the ^{3}He counters for detecting neutrons of different energies was calibrated above 80 keV against that of a methane (CH_4)-filled proportional counter and, at lower energies, against that of another gas counter filled with $^{10}BF_3$. Consequently, the measured energy variation of the neutron flux, and hence the shape of the excitation function for radiative capture, is based upon the cross section* for the $^{10}B(n, \alpha_0 + \alpha_1\gamma)^7Li$ reaction at neutron energies below 80 keV and upon the n+p scattering cross section [4] at higher energies. These cross sections are widely considered to be the best standards presently available for partial neutron cross-section measurements at these energies.

To supplement the flux data obtained from the ^{3}He monitor counters, separate measurements of the flux were made either before or after a capture determination with the methane counter placed in the centre of the neutron beam near the liquid scintillator. These measurements have an overall resolution of 3 ns/m (about four times better than the ^{3}He measurements) and provide more detailed information on the neutron spectrum at higher energies. The ^{3}He monitors were also used during the measurements with the methane counter to verify that the flux spectrum was the same as that observed during the capture measurements. The flux data from the methane counter were used at energies above 80 keV.

For all three types of proportional counters used in this work, the corrections made for backgrounds, self-shielding and multiple scattering in the gas, transmission through end windows, and wall-scattering and misalignment effects are well understood and were kept small. The active volume of the counters and their timing resolution were determined experimentally. Full details of the construction and instrumentation of these counters are given in Ref. [5].

The methane counter was implemented for time-of-flight measurements by using a computer-based data acquisition system [6] to record both the pulse height and neutron flight time associated with each event in the counter. Pulse-height spectra from the methane counter for four flight-time intervals are shown in Fig. 2. The solid curves in the figure are the results of Monte Carlo calculations [7] of the proton-recoil spectrum which were made to extrapolate the spectra to zero pulse

*This cross section was taken to vary as (1/v) from the thermal value [2] to 80 keV.

height. The spectrum for a given interval of flight time is summed only above a threshold pulse height (see broken lines in Fig. 2) taken at three-tenths of the maximum proton-recoil pulse height, which eliminates the smaller pulses due to ^{12}C recoils. The relative efficiency of the counter, which then varies little with incident neutron energy, is established directly from the fraction of the proton-recoil spectrum that lies above the threshold pulse height. The implementation of the ^{3}He and $^{10}BF_3$ counters is more straightforward since a fixed electronic threshold can be used that will eliminate ^{3}He and ^{10}B recoils, respectively, at all neutron energies of interest. Some two-parameter (pulse-height and time-of-flight) data were also taken for the ^{3}He counter to determine the $^{3}He(n, p)T$ cross section relative to the ^{3}He total cross section in the neutron energy region 0.3 to 1.16 MeV [8].

Neutron flux data with an overall uncertainty of about 5% in relative intensity were obtained routinely over the neutron energy region ~100 eV - 1 MeV. A typical time-of-flight flux spectrum is shown in Fig. 3. Although absolute flux data are illustrated in this figure, only the relative energy variation (or time history) of the incident flux is required in our experiment. Normalisation of the radiative capture yields is discussed in the next Section.

2.2. Capture yields

For most of the data reported here, a 600-litre liquid scintillator viewed by photomultipliers (illustrated in Fig. 1) was used to detect the capture gamma rays. This scintillator has recently been enlarged to a volume of 2400 ℓ to improve the signal-to-background ratio by increasing the efficiency for summing capture γ-ray cascades. This improvement was particularly important in the measurements for ^{238}U due to the low excitation energy (~ 4.8 MeV) of the compound nucleus. Both scintillator configurations used in this work were similar in construction to that described in Ref. [9].

The photomultiplier outputs were summed to produce a pulse proportional to the total γ-ray energy deposited in the liquid. A pulse-height window discriminator was normally set to accept events depositing a total energy in the range 4 to 10 MeV, and the time history of accepted events was stored by a multi-channel analyser. In recent measurements made with the enlarged scintillator, three types of data were obtained simultaneously. Two data channels used different lower limits (3.5 and 4.5 MeV) for the discriminator and provided a useful check on the variation of the detection efficiency with neutron energy (see below). In the third data channel a 3.5-MeV level was used, but a coincidence was required which assured that at least 1 MeV of energy was deposited in each of the two optically isolated halves of the scintillator. This requirement selects many of the multi-gamma cascades which are usually produced by capture and eliminates many single-gamma events that are usually associated with background. This increased the signal-to-background ratio

by about one order of magnitude, and comparison of the data taken for several samples both with and without the coincidence requirement has failed to reveal any dependence on the γ-ray cascade mode (or energy spectrum) introduced by the requirement. Moreover, the γ-ray energy spectrum is not expected to vary markedly with neutron energy when the measurement averages over many resonances of the compound nucleus. Figure 4 illustrates the very acceptable signal-to-background ratio achieved with the coincidence mode for ^{238}U, which has the poorest signal-to-background ratio of the nuclei measured here. Gain shifts in each data channel were checked by verifying a constant (flight-time independent) difference of counts between capture yields measured with and without a ^{24}Na γ-ray source placed near the sample but outside the neutron beam. This difference (the count rate from the ^{24}Na source) is very sensitive to gain shifts since the total γ-ray energy from ^{24}Na is close to the sum-signal discriminator threshold.

The ambient background shown in Fig. 4 is the constant background arising principally from cosmic-ray interactions with the scintillator. The sample-out background varies with neutron flight time and is primarily due to neutrons scattered and captured in the vicinity of the collimator nearest to the scintillator. The scattered-neutron background results from neutrons scattered by the sample and then captured in the scintillator materials. A measure of this background was obtained by substituting a lead or carbon sample (where capture is negligible) and scaling the observed γ-ray counts by the ratio of scattering probabilities at a representative neutron energy that takes into account the mean lifetime of neutrons in the scintillator. An overall check of the background subtractions is made by introducing a thick sodium "notch" filter in the beam ahead of the capture sample. The count rate observed at the bottom of the transmission dip at the 2.85-keV resonance in $^{23}Na+n$ has always agreed within a few percent with the sum of the individually determined backgrounds. The statistical precision of the net capture counts (summed over 5% energy intervals under 50 keV) is ±10% or better for all elements at all neutron energies.

A typical capture yield (net capture counts divided by the incident neutron flux) obtained for gold with the 230-m flight-path facility is shown by the points in the upper portion of Fig. 5. The data are usually taken with a 2-μs accelerator burst width and a 2-μs channel width for the time analyser, which results in an overall energy resolution of about 1% at 1 keV and 20% at 1 MeV. The data extend downward in neutron energy to about 70 eV, and known [2] resonances in $^{197}Au+n$ below 300 eV are indicated in the figure. When accurate resonance parameters are available, the yields can be normalised from the observed and calculated areas of capture resonances in the energy region ~100 eV. By scaling the measured yield to produce the calculated area, the capture probability for a given sample thickness can be normalised without recourse to a determination of the absolute detection efficiency for either the capture γ-rays or the incident neutrons.

To improve the precision of the normalisation, capture yields at lower neutron energies were measured for each sample with a 20-m neutron flight-path facility using a 4000-ℓ scintillator [9] to detect the capture γ-rays and a ^{3}He gas proportional counter to detect the incident neutrons. Data were obtained with this facility from about 2 eV - 20 keV, and the results for Au are shown in the lower portion of Fig. 5. At these lower energies most of the elements studied have resonances that, for the sample thickness used, become "saturated"; i.e. they have a neutron interaction probability near unity. When the resonance is also weak ($\Gamma_n << \Gamma_\gamma$), the area of the resonance calculated near its peak then becomes essentially independent of the values of the resonance parameters, and the yields measured with the 20-m facility can be normalised with an accuracy of 1-2%. The yields determined with the 230-m facility were then normalised to the absolute 20-m results in the region where the two data sets overlap. This is normally done by matching the integrals of the yields from 2-8 keV, as is indicated in the figure.

Typical fits to saturated resonances are shown in Fig. 6 for ^{197}Au(n, γ) and ^{238}U(n, γ). The resonance shapes were calculated with a Monte Carlo code [10] that includes Doppler and resolution broadening, multiple neutron scattering, and incoherent contributions from adjacent resonances. Existing resonance parameters were used without any adjustment to produce detailed fits in the wings of the resonances, and the calculated capture probabilites were used only at energies near the peak of the resonance. In most cases several resonances of a given nuclide, although not saturated, were suitable for normalisation; and the absolute yield could therefore be determined at more than one energy. This provides a check on the flux spectrum measured at low energies, as is illustrated in Fig. 7. The curve in this figure was obtained from a least-squares fit to the flux data measured with the ^{3}He counters, and the points denote the relative flux deduced from the ratio of observed and calculated capture areas of eight resonances in ^{181}Ta+n. The normalisation of the yields for Rh, Ta, Au and ^{238}U measured with the 230-m flight path is judged to be determined within ± 5%.

Normalisation of the yields for Mo, Gd, W, and Re is less straightforward since the effective γ-ray detection efficiency for samples that are not essentially monoisotopic involves an average of the different efficiencies for each isotope weighted by both the isotopic abundance and the average isotopic capture cross section. The latter were taken from recent data and, in some cases, were estimated from statistical-model calculations. An additional difficulty is present for the molybdenum isotopes, where existing resonance parameters produced very poor agreement with many of the observed capture resonances, and where none of the resonances was saturated for a sample thickness of 0.25 cm. This difficulty was partially overcome by comparing capture γ-ray pulse-height distributions for resonances in different isotopes and deducing relative detection efficiencies from the observed spectrum fractions above the discriminator threshold. Full details of the normalisation are

given in Ref. [11] for Gd, Ref. [5] for W and Re, and Ref. [12] for Mo. The normalisation of the yield is judged to be determined to within ±10% for Gd, W, and Re and within ± 20% for Mo.

The average capture cross sections were obtained from the normalised yields measured with the 230-m flight path facility by taking into account the variation of γ-ray detection efficiency at the higher incident neutron energies and the finite-sample effects of multiple scattering and self-shielding. For all samples the capture data obtained with no coincidence requirement were used at the higher energies, and the efficiency variation was calculated from the change in the spectrum fraction of scintillator pulses above the sum-signal discriminator threshold. The pulse-height distributions at high energies were deduced from those measured in the resolved-resonance region with the assumption that the distribution is stretched linearly with the initial excitation energy of the compound nucleus. (The spectra $f(E_\gamma)$ measured at low neutron energies were replaced by the spectra $g(E_\gamma) = f[E_\gamma B_n/(B_n + E_n)]$, where E_γ is the γ-ray energy, B_n the neutron separation energy, and E_n the incident neutron energy.) For multi-isotopic samples, the efficiency correction was obtained from an average weighted by isotopic capture cross sections. At 700-keV incident energy, this correction was ~10% or less for all samples except ^{238}U, where it was about 20%. Corrections for resonance self-shielding and multiple scattering were determinted with the code SESH [13] which uses Monte Carlo methods to generate a Doppler-broadened resonance environment at each collision in the sample. This environment is produced by sampling distributions of resonance widths and spacings calculated from specified values of neutron strength functions, average level spacings, and average radiation widths. The total correction to the data for finite-sample effects was ⩽15% for all samples at neutron energies above 5 keV.

3. RESULTS

Our capture cross-section results for Mo, Rh, Gd, Ta, W, and Re are shown in Fig. 8 together with some previous data from other laboratories. The other data chosen for illustration were selected somewhat at random. The data of Gibbons et al. [14] and Diven et al. [15] are perhaps representative of "early" (1960-62) measurements made with liquid scintillators and pulsed van de Graaff neutron sources. The data of Kompe [16] obtained with a liquid scintillator and van de Graaff, and those* of Moxon [17] measured with a Moxon-Rae detector and electron linear accelerator, have been published within the last two years. A variety of neutron flux measurement techniques and capture-yield

*The data of Ref. [17] are measured at very small energy intervals, and many of these points are not included in Figs. 8 and 9.

normalisation procedures are represented, and several primary and secondary cross-section standards are involved.

Of our present results for eight elements, those for Mo(n, γ) appear to be in poorest agreement with previous data. The data of Weigmann and Schmid [18] are relative to $^{10}B(n, \alpha)^{7}Li^{*}$ and are normalised to saturated resonances in Ag, and these results agree well with those of Kompe [16] which are relative to the Au(n, γ) data of Poenitz et al. [3] (discussed below). The data of Mitzel and Plendl [19] are relative to $^{10}B(n, \alpha)$ and are normalised to Mo resonances. Even in view of some uncertainties in both the present and previous data which arise from poor resonance-parameter and isotopic cross-section information, it is difficult to account for the systematically smaller cross sections found here at the lower energies. Further measurements designed to definitively resolve these discrepancies for Mo(n, γ) are planned at this laboratory.

Our cross sections for Rh are about 20% higher (at least in the region 10-50 keV) than those determined by Moxon [17], which are relative to $^{10}B(n, \alpha)^{7}Li^{*}$ and normalised to saturated resonances. The present data for Gd near 100 keV do not fall off as fast with increasing neutron energy as those of Gibbons et al. [14], which are relative to their determination [14] of the excitation function for In(n, γ). A similar disagreement with the results of Gibbons et al. occurs for Ta and Au. Agreement of our Ta data with the other results illustrated is exceptionally good at all energies below 900 keV. Discrepancies in the average cross section exceed a few percent only in the region ~ 50-150 keV, where our results are ~ 10% higher than those of Kompe [16] and ~ 20% higher than those of Moxon [17].

Our data for W are ~ 20% lower than those of Kompe below 100 keV and are also lower than those of Gibbons et al. both below 20 keV and above 100 keV. The vast disagreement above 100 keV with the measurements of Diven et al. [15] relative to the ^{235}U capture-plus-fission cross section is not easily explained. Similar but smaller disagreements with the results of that experiment are also observed for Mo, Ta, W and ^{238}U but do not appear to be present for Rh and Au. Our excitation function for Re disagrees in shape with that measured by Kononov and Stavisskii [20] relative to the In(n, γ) cross section determined by Gibbons et al. Our Re data are about 10% lower than those of Kompe below 50 keV and about 20% lower than the results of Block [21], which are all at energies < 10 keV. The latter measurements were made relative to $^{10}B(n, \alpha)$ but were normalised without a detailed consideration of the capture γ-ray detection efficiency.

Capture data for Au and ^{238}U are shown in Fig. 9. Our data for gold agree within a few percent at all energies below 400 keV with the measurements of Poenitz et al. [3] made with a "grey" (flat-response) neutron detector and normalised at 30 keV to an absolute value of the

cross section determined by five independent measurements. The cross section measured by Poenitz et al. at ~470 keV is about 10% lower than our data. Our data from ~40-200 keV are about 20% higher than the data of both Gibbons et al. and the later measurements of Macklin and Gibbons [22], which are relative to their previous results for Ta, In or I. Except near 500 keV, our data for Au(n, γ) are 10-20% lower than the activation measurements of Cox [23], which are relative to $^{10}B(n, \alpha)$ below 200 keV and based on $^{235}U(n, f)$ above 200 keV. Our data above 400 keV are ~ 15% higher than the absolute activation measurements of Harris [24] and agree closely above 400 keV with the measurements of Grench and Vaughn [2] relative to $^{235}U(n, f)$. Our gold data from 200-800 keV also agree within ~10% with the measurements of Barry [25] using a ^{235}U fission counter calibrated [1] against the n+p cross section.

Our data for ^{238}U are once again in best overall agreement with measurements by Menlove and Poenitz [26] using the grey detector and an absolute activation normalisation at 30 keV. Our results are somewhat lower than the evaluation of Davey [27] below 20 keV, and ~15% lower everywhere in the region 200-800 keV. The cross sections above 200 keV recommended by Davey are essentially equivalent to the activation measurements of Barry [28], which were relative to the ^{235}U fission cross section. Our results near 40 keV are about 20% higher than the data of Moxon [17], which were obtained relative to $^{10}B(n, \alpha)^{7}Li^{*}$ and were normalised to saturated resonances.

4. CONCLUSIONS

With the possible exception of the results for Mo(n, γ), the present measurements considered together with previous data obtained over more limited regions of energy are believed to establish the absolute average capture cross sections discussed here to within 10-15% over the full energy region ~ 1-1000 keV. The present experiment is designed to yield cross-section values with an accuracy ~10% over a very large energy range. Consequently, it is difficult to judge whether our results lend support to previous indications that gold capture data based on the ^{235}U fission cross section are ~ 15% higher than other results above 200 keV. Our data for gold above 400 keV are in good agreement with one such measurement by Grench [2] and yet are also in good agreement with the data of Poenitz et al. [3] at lower energies. Our cross sections for $^{238}U(n, \gamma)$ agree best with those of Menlove and Poenitz [26], are consistently smaller above 200 keV than the recommended values of Davey [27], and do not support the lower capture cross sections obtained by Moxon [17] between 20 and 100 keV.

REFERENCES

[1] White, P. H., J. Nucl. Energy 19 (1965) 325.

[2] Brookhaven National Laboratory Report BNL 325, 2nd ed., Supplement 2 (1964-66).

[3] Poenitz, W. P., et al., J. Nucl. Energy 22 (1968) 505.

[4] Gammel, J. L., "The n-p Total and Differential Cross Sections in the Energy Range 0-40 MeV," Ch. V. T, Fast Neutron Physics, Part II (Marion, J. B., and Fowler, J. L., Eds.), Interscience, New York (1963).

[5] Lopez, W. M., et al., National Aeronautics and Space Administration Report NASA CR-72474 (1968).

[6] Lopez, W. M., Proceedings for the Skytop Conference on Comp ter Systems in Experimental Nuclear Physics, Conf - 690301, EANDC (U.S.) 121 u (1969).

[7] Parker, J. B., et al., Nucl. Instr. and Methods 23 (1963) 61.

[8] Costello, D. G., et al., Nucl. Sci. and Engr. 39 (1970) 409.

[9] Haddad, E., et al., Nucl. Instr. and Methods 31 (1964) 125.

[10] Fröhner, F. H., Gulf General Atomic Report GA-6906 (1966).

[11] Fricke, M. P., et al., USAEC Report GA-9275 (1969).

[12] Friesenhahn, S. J., et al., Gulf General Atomic Report GA-10081 (1970).

[13] Fröhner, F. H., Gulf General Atomic Report GA-8380 (1968).

[14] Gibbons, J. H., et al., Phys. Rev. 122 (1961) 182.

[15] Diven, B. C., et al., Phys. Rev. 120 (1960) 556.

[16] Kompe, D., Nucl. Phys. A133 (1969) 513.

[17] Moxon, M. C., "The Measurement of Average Neutron Capture Cross Sections in the Mass Region Above 100," thesis-London University, July 1968, HL68/3739.

[18] Weigmann, H., and Schmid, H., Nucl. Phys. A104 (1967) 513.

[19] Mitzel, V. F., and Plendl, H. S., Nukleonik 6 (1964) 371.

[20] Kononov, V. N., and Stavisskii, Yu. Ya., Atomnaya Energiya 19 (1965) 457.

[21] Block, R. C., et al., "Neutron Radiative Capture Measurements Utilizing a Large Liquid Scintillator Detector at the ORNL Fast Chopper," Neutron Time-of-Flight Methods (Saclay Conf.) (Spaepen, J., Ed.), EURATOM (1961).

[22] Macklin, R. L., and Gibbons, J. H., Phys. Rev. 159 (1967) 1007.

[23] Cox, S. A., Phys. Rev. 122 (1961) 1280.

[24] Harris, K. K., et al., Nucl. Phys. 69 (1965) 37.

[25] Barry, J. F., J. Nucl. Energy 18 (1964) 491.

[26] Menlove, H. O., and Poenitz, W. P., Nucl. Sci. and Engr. 33 (1968) 24.

[27] Davey, W. G., Nucl. Sci. and Engr. 39 (1970) 337.

[28] Barry, J. F., et al., J. Nucl. Energy 18 (1964) 481.

FIGURE CAPTIONS

Fig. 1. Facility for capture cross-section measurements.

Fig. 2. Proton-recoil pulse-height spectra from methane gas proportional counter. The solid curves are the results of Monte Carlo calculations [7], and the broken lines denote the threshold pulse heights described in the text.

Fig. 3. Neutron flux per unit time of flight measured with ^{3}He and methane proportional counters.

Fig. 4. Time-of-flight neutron capture data and γ-ray backgrounds described in the text.

Fig. 5. Capture probabilities measured with 230-m and 20-m neutron flight paths. The scatter of points is primarily due to partially-resolved resonance structure.

Fig. 6. Data and calculations for saturated resonances in gold and uranium.

Fig. 7. Flux normalisation deduced from eight resonances in tantalum. The curve was obtained from a least-squares fit to the flux data and was normalised to three saturated resonances below 15 eV.

Fig. 8. Capture data for Mo, Rh, Gd, Ta, W, and Re.

Fig. 9. Capture data for Au and ^{238}U.

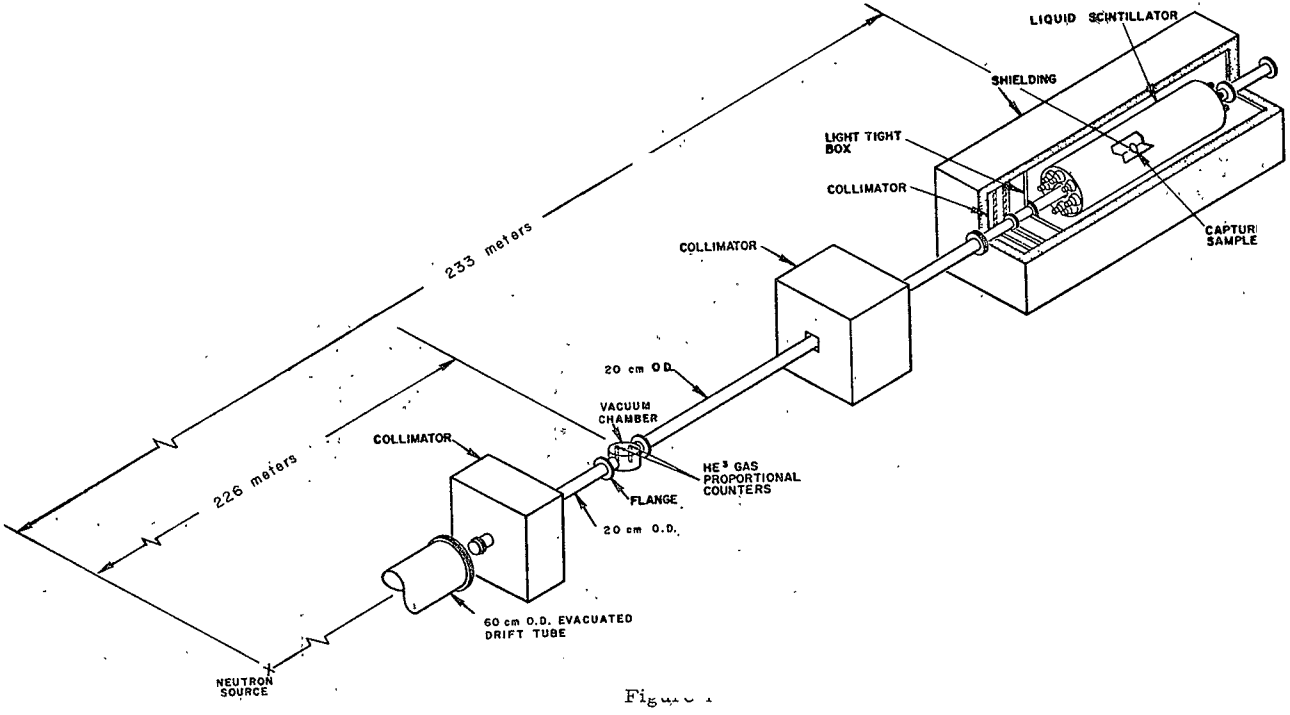
LIQUID SCINTILLATOR
SHIELDING
LIGHT TIGHT BOX
COLLIMATOR
CAPTURE SAMPLE
COLLIMATOR
233 meters
20 cm O.D.
VACUUM CHAMBER
COLLIMATOR
226 meters
HE³ GAS PROPORTIONAL COUNTERS
FLANGE
20 cm O.D.
60 cm O.D. EVACUATED DRIFT TUBE
NEUTRON SOURCE

Figure 1

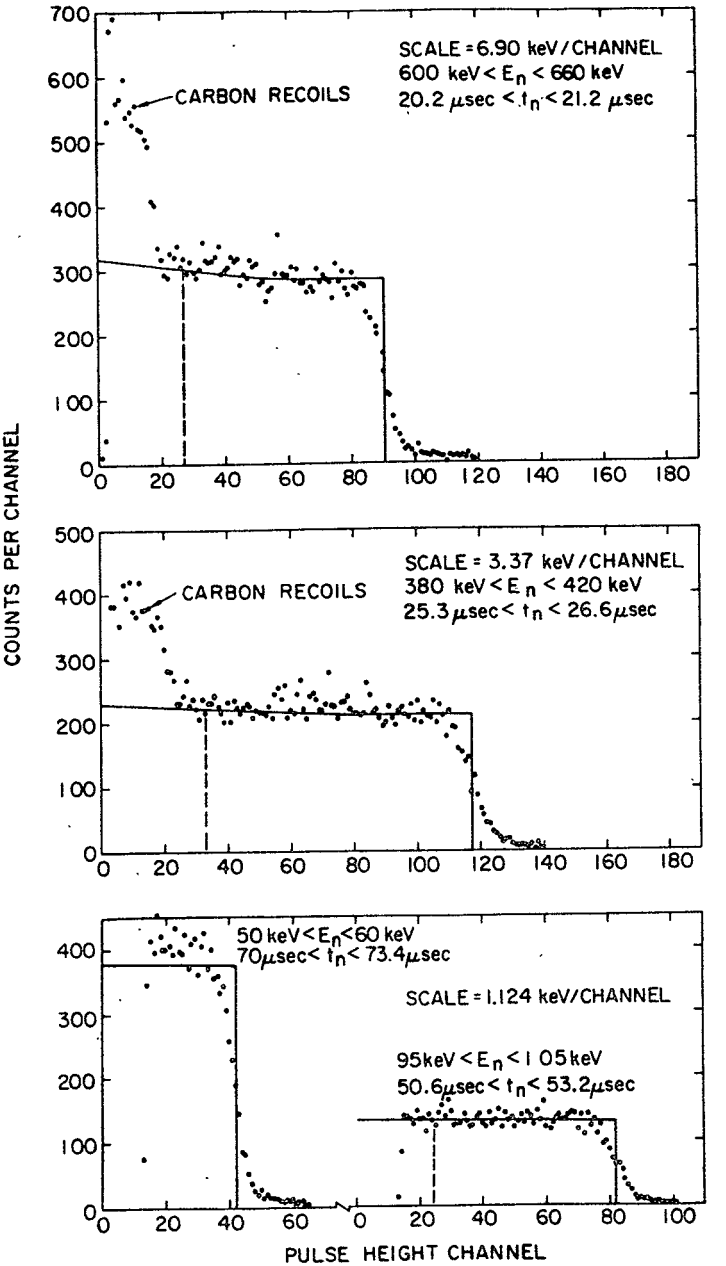
SCALE = 6.90 keV/CHANNEL
600 keV < E_n < 660 keV
20.2 μsec < t_n < 21.2 μsec
CARBON RECOILS
SCALE = 3.37 keV/CHANNEL
380 keV < E_n < 420 keV
25.3 μsec < t_n < 26.6 μsec
CARBON RECOILS
50 keV < E_n < 60 keV
70 μsec < t_n < 73.4 μsec
SCALE = 1.124 keV/CHANNEL
95 keV < E_n < 105 keV
50.6 μsec < t_n < 53.2 μsec
COUNTS PER CHANNEL
PULSE HEIGHT CHANNEL

Figure 2

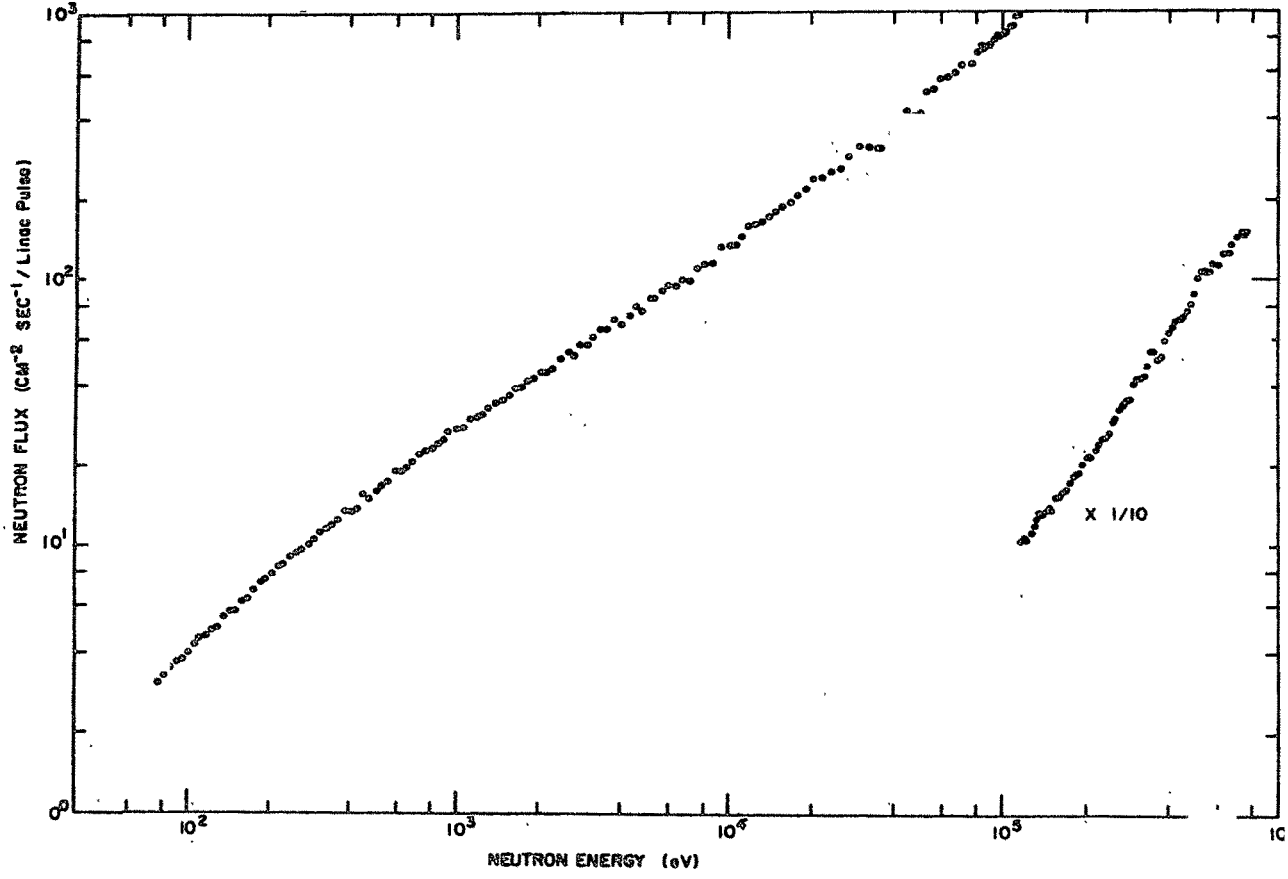

Figure 3

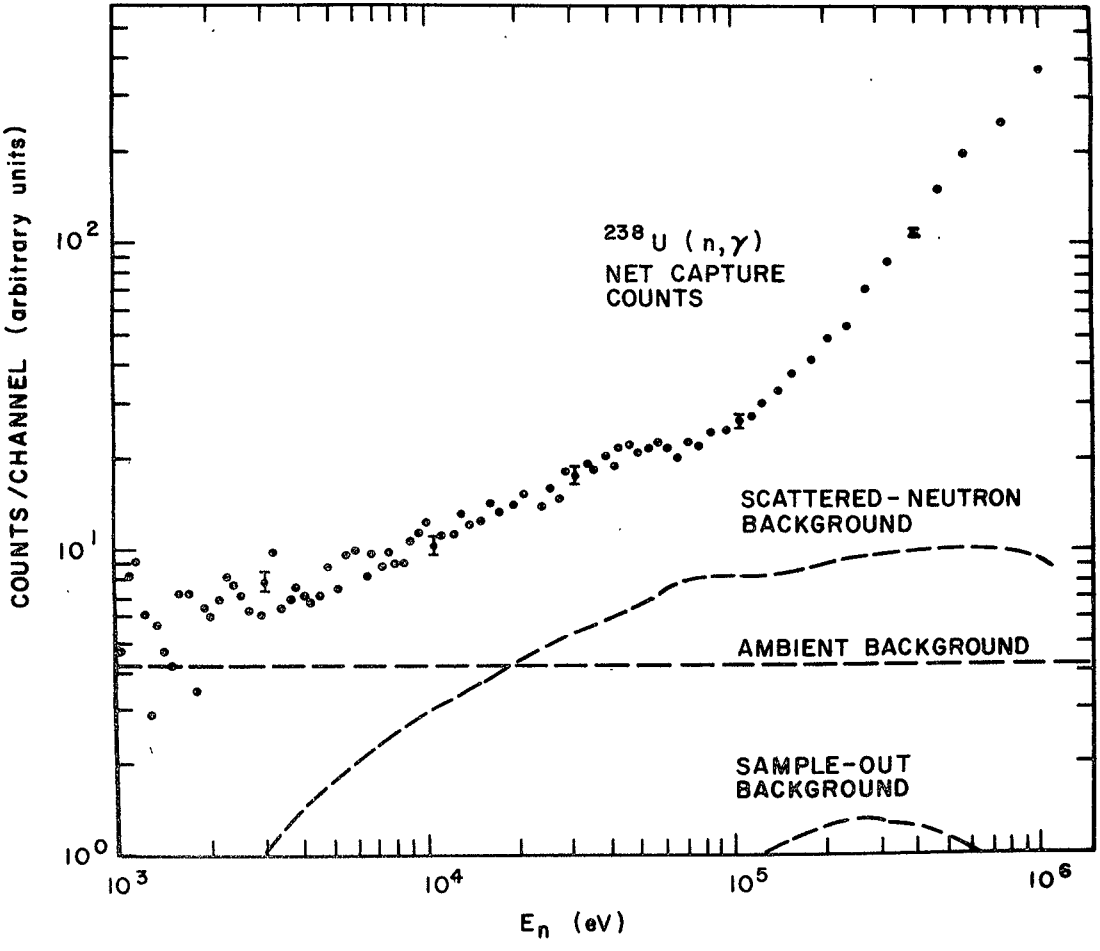
COUNTS/CHANNEL (arbitrary units)
10^2
10^1
10^0
^{238}U (n,γ)
NET CAPTURE
COUNTS
SCATTERED-NEUTRON
BACKGROUND
AMBIENT BACKGROUND
SAMPLE-OUT
BACKGROUND
10^3
10^4
10^5
10^6
E_n (eV)

Figure 4

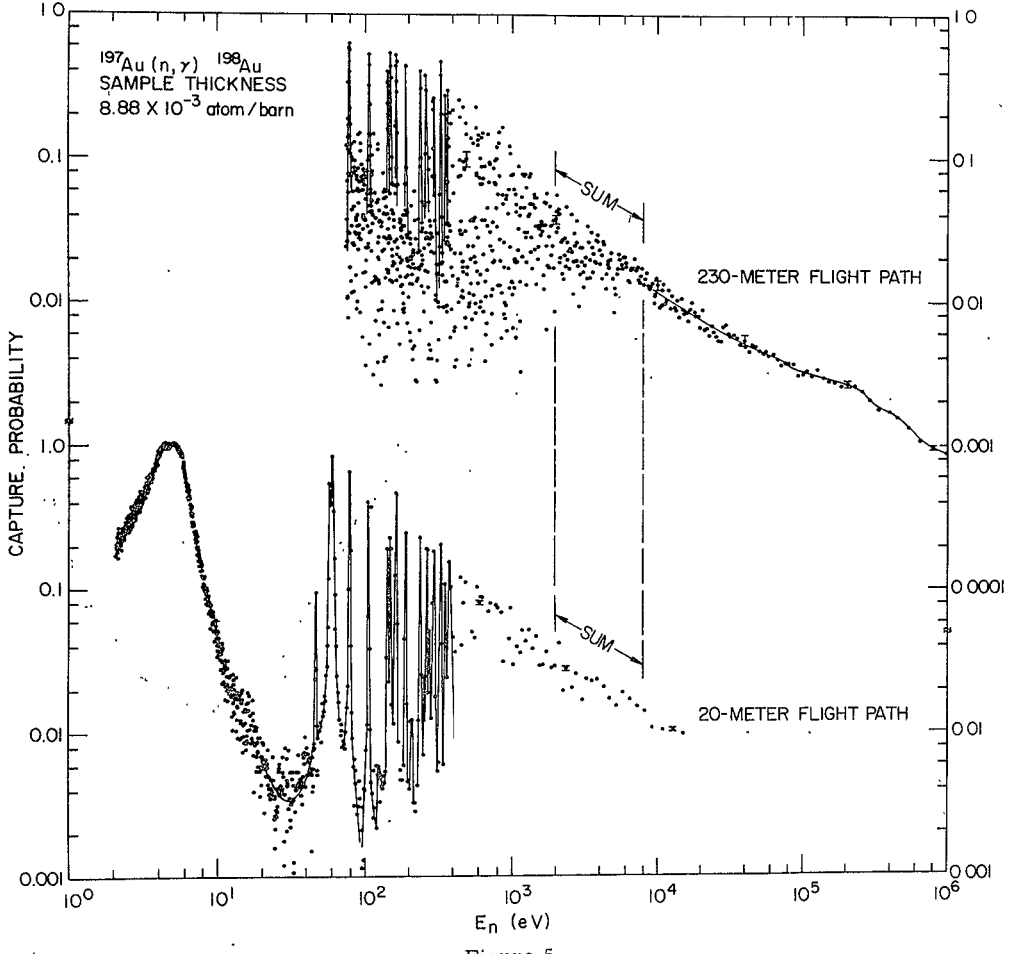
197Au (n, γ) 198Au
SAMPLE THICKNESS
8.88 X 10-3 atom/barn
SUM
230-METER FLIGHT PATH
SUM
20-METER FLIGHT PATH
CAPTURE. PROBABILITY
En (eV)
1.0
0.1
0.01
0.001
0.0001
10^0
10^1
10^2
10^3
10^4
10^5
10^6

Figure 5

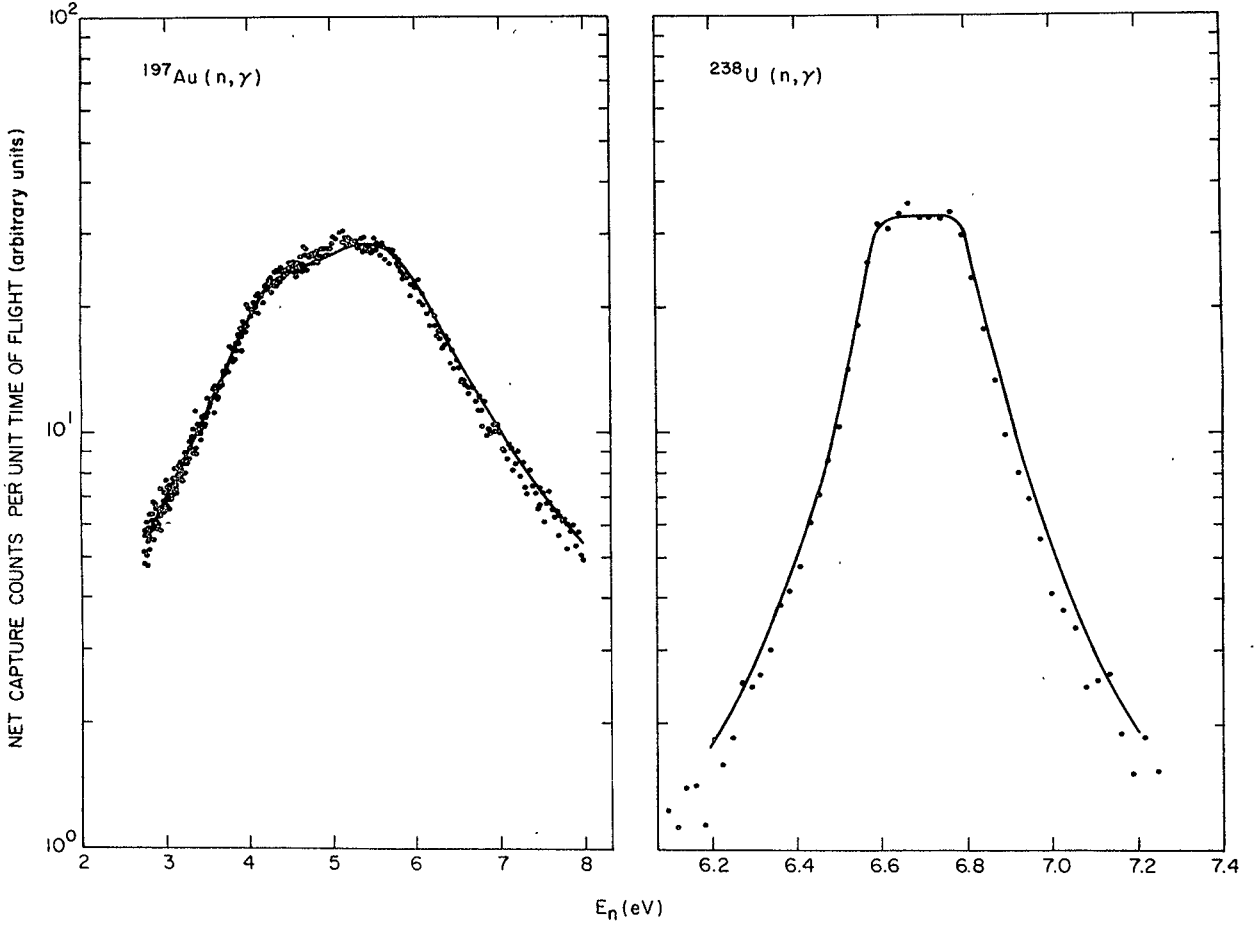
^{197}Au (n,γ)
^{238}U (n,γ)
NET CAPTURE COUNTS PER UNIT TIME OF FLIGHT (arbitrary units)
10^2
10^1
10^0
2
3
4
5
6
7
8
6.2
6.4
6.6
6.8
7.0
7.2
7.4
E_n(eV)

Figure 6

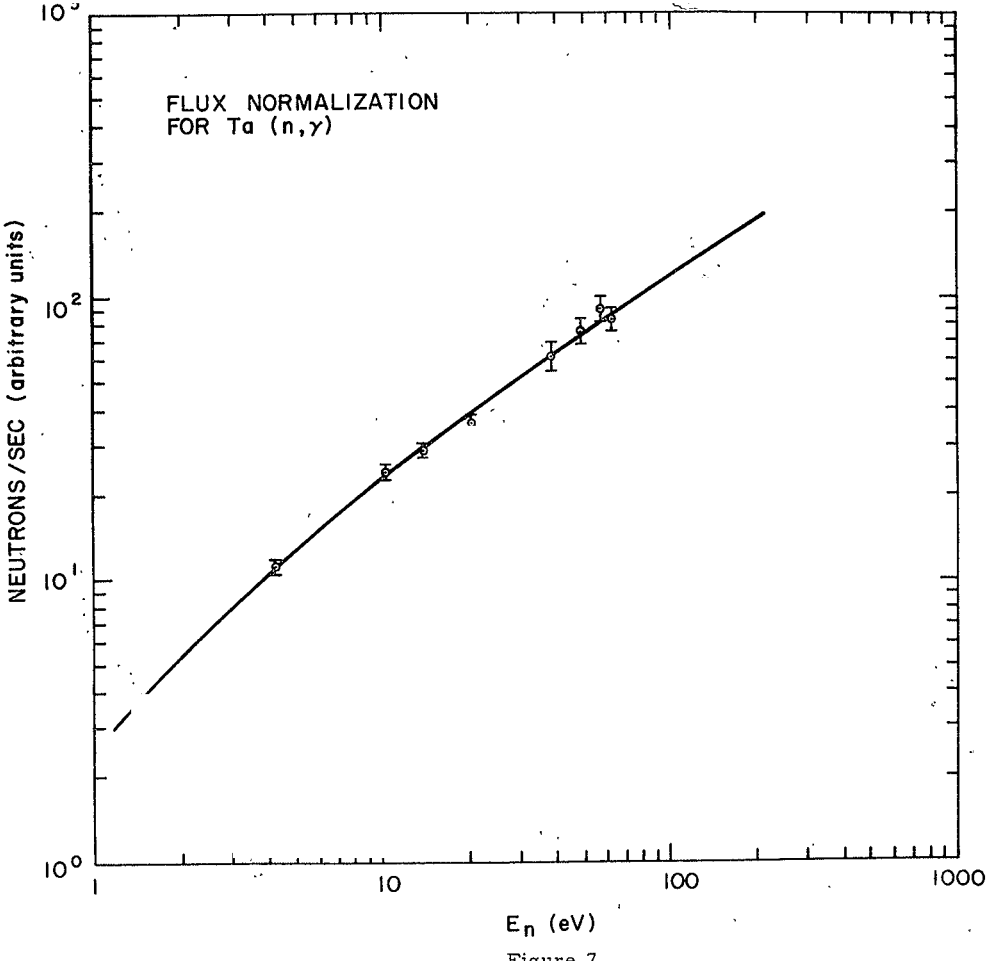
FLUX NORMALIZATION
FOR Ta (n,γ)
NEUTRONS/SEC (arbitrary units)
10^2
10^1
10^0
1
10
100
1000
E_n (eV)

Figure 7

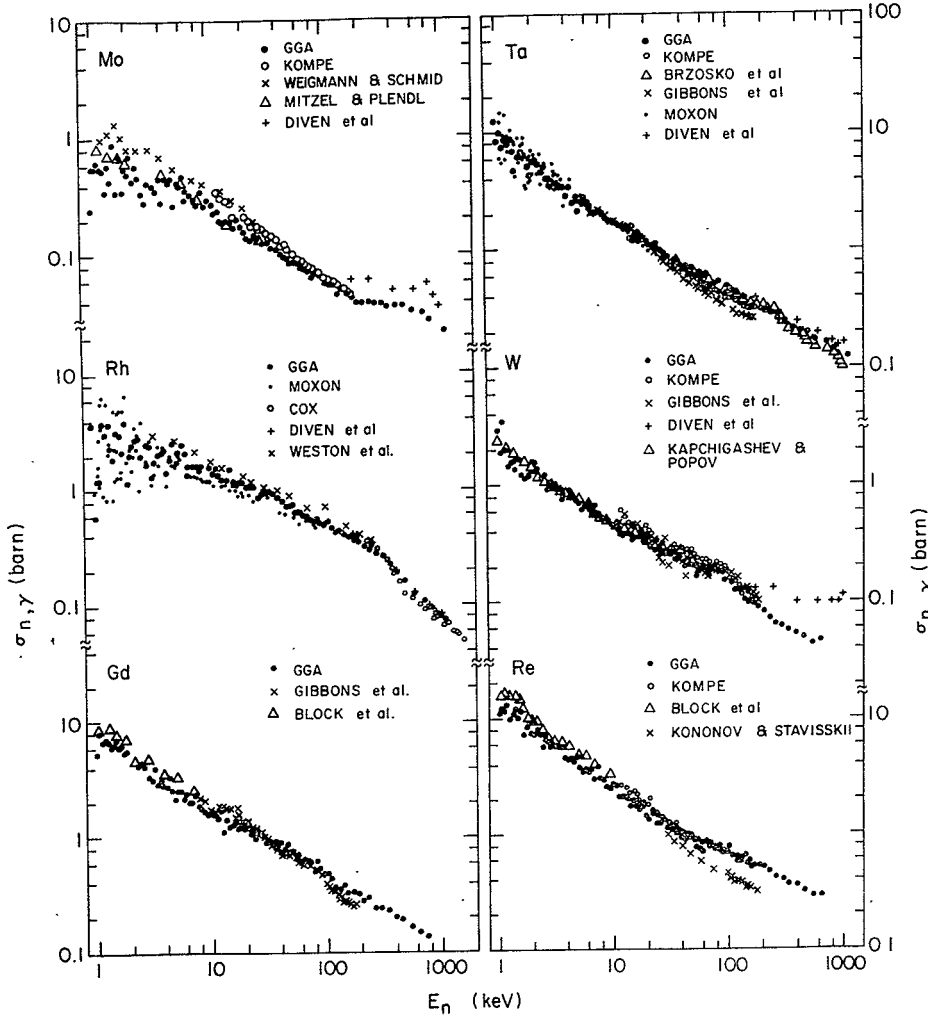
Mo
GGA
KOMPE
WEIGMANN & SCHMID
MITZEL & PLENDL
DIVEN et al
Ta
GGA
KOMPE
BRZOSKO et al
GIBBONS et al
MOXON
DIVEN et al
Rh
GGA
MOXON
COX
DIVEN et al
WESTON et al.
W
GGA
KOMPE
GIBBONS et al.
DIVEN et al
KAPCHIGASHEV & POPOV
Gd
GGA
GIBBONS et al.
BLOCK et al.
Re
GGA
KOMPE
BLOCK et al
KONONOV & STAVISSKII
σn,γ (barn)
En (keV)

Figure 8

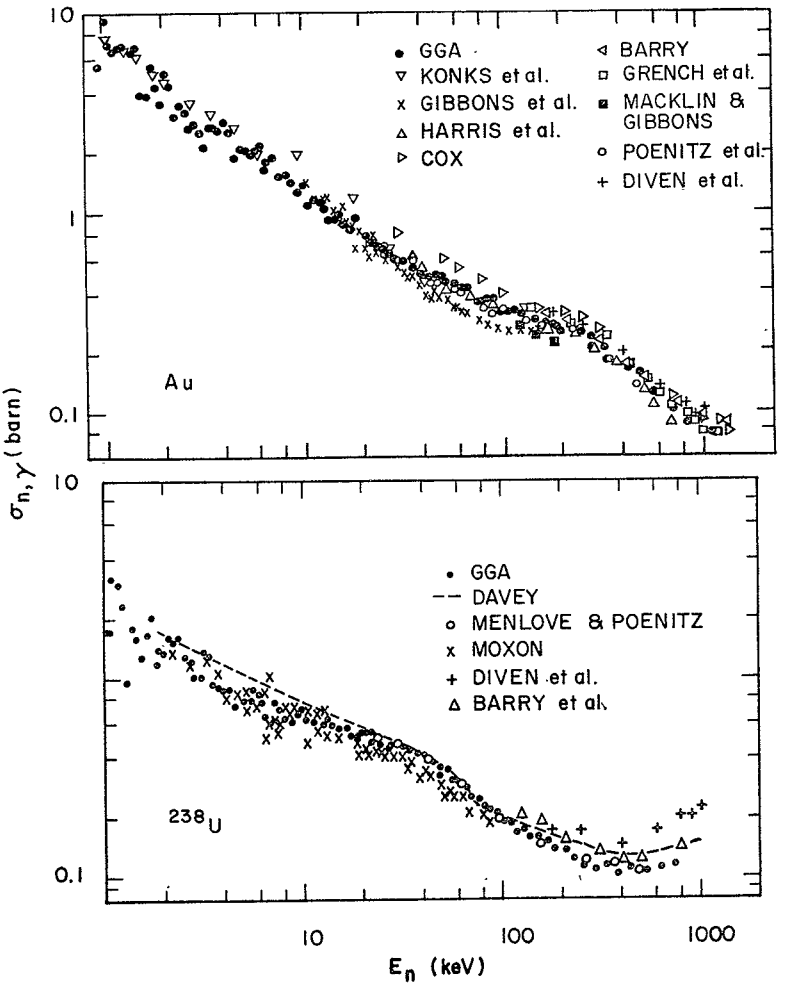
10
1
0.1
Au
GGA
KONKS et al.
GIBBONS et al.
HARRIS et al.
COX
BARRY
GRENCH et al.
MACKLIN & GIBBONS
POENITZ et al.
DIVEN et al.
10
0.1
238U
GGA
DAVEY
MENLOVE & POENITZ
MOXON
DIVEN et al.
BARRY et al.
10
100
1000
En (keV)
σn,γ (barn)

Figure 9

Calculations of Cross Sections for the Radiative Capture of Fast Neutrons*

M. P. Fricke, W. M. Lopez,+ S. J. Friesenhahn
A. D. Carlson and D. G. Costello

Gulf General Atomic Incorporated
San Diego, California 92112, USA

The data of the previous paper (CN-26/43), together with some results of recent activation measurements, have been analysed in terms of the statistical model. It has not been found possible to reproduce most of the observed excitation functions using the customary energy dependence of the γ-ray penetrabilities. This result is independent of (1) different optical-model parameters used to describe the neutron channels and the effects of a non-spherical potential; (2) different level-density formulas and a wide variation in their parameters; (3) extreme assumptions of neutron width-fluctuation correlations; (4) extreme limits of the effect of the $(n, \gamma n')$ process; and (5) of any plausible spin or parity dependence of the total radiation width. If the usual form is retained for the γ-ray penetrabilities, $T_\gamma \sim 2\pi \langle \Gamma_\gamma \rangle / D$, then the most likely source of difficulty appears to lie with the conventional excitation-energy dependence of the average partial radiation widths that sum to $\langle \Gamma_\gamma \rangle$.

---

*Work supported in part by the U. S. Atomic Energy Commission.

+Present address: University of California at San Diego, La Jolla, California 92037, USA.

Calculations of Cross Sections for the Radiative Capture of Fast Neutrons*

M. P. Fricke, W. M. Lopez,+ S. J. Friesenhahn
A. D. Carlson and D. G. Costello

Gulf General Atomic Incorporated
San Diego, California 92112, USA

1. INTRODUCTION

Reliable experimental information on average neutron capture cross sections, particularly at energies ≥ 100 keV, is virtually absent for some important fertile and fissile nuclei and completely absent for most fission-product nuclides. This places considerable emphasis on theoretical capabilities to predict these cross sections or to extrapolate them from energies where credible measurements have been made. For a critical examination of such capabilities, it is desirable to consider first the case where fission channels are closed.

The current theoretical description of average capture cross sections below one MeV was developed quite fully almost two decades ago [1]. The Hauser-Feshbach theory is used, and the shape of the excitation function for capture is fairly insensitive to different optical-model characterisations of the neutron channels. The main ingredient for capture cross sections is the radiative strength function, i.e. the ratio of the average total radiation width to the average level spacing. The average radiation width is calculated conventionally from the Weisskopf estimate [2], and the average level spacing is taken from standard level-density formulas. When radiation widths and level

* Work supported in part by the U. S. Atomic Energy Commission.

+ Present address: University of California at San Diego, La Jolla, California 92037, USA.

spacings have been measured for low-energy neutron resonances, or when the average capture cross section is known in the lower-keV region, the radiative strength function can be chosen to produce agreement with these data. The average capture cross section at higher energies is then determined principally by the variation of the radiative strength function with energy.

Such calculations have been compared to the data presented in the previous paper (CN-26/43) and also to recent measurements by Stupegia et al. [3]. We conclude that the conventional treatment of the capture reaction is in general unable to reproduce the observed excitation functions in the region ~ 100 keV - 1 MeV. Early results of this study were presented in Ref. [4].

2. THEORY

The average angle-integrated compound-nucleus cross section is given [5] by the following sum over all entrance (α) and exit (β) channel quantum numbers:

$$\sigma_{n,x} = \pi \lambda^2 \Sigma_{\alpha\beta} g_\alpha^J [F_{\alpha\beta} \langle \theta_{\mu\alpha} \rangle \langle \theta_{\mu\beta} \rangle / \langle \theta_\mu \rangle - \delta_{\alpha\beta} Q_\alpha \langle \theta_{\mu\alpha} \rangle^2 / 4]. \quad (1)$$

Here g_α^J is the spin statistical factor; $F_{\alpha\beta}$ the correction for width fluctuations; and $\langle \theta_\mu \rangle$ is a sum over all open channels ν of resonance parameters $\langle \theta_{\mu\nu} \rangle$, where the brackets denote an average over compound levels μ.

The average resonance parameters for the neutron channels are

the excitation function from 100 keV - 1 MeV is incorrectly reproduced; the calculated capture cross sections fall off too slowly with increasing neutron energy, even with the maximum effect of (n, γn'). We note that this discrepancy is opposite to that found at much higher energies, $E_n \geq 10$ MeV, where a direct or collective capture mechanism is required to increase the calculated cross sections above those given by the compound-nucleus treatment. The discrepancy found here was also observed in the previous work of Stupegia et al. [3]. Of the nuclei examined in that study, the discrepancy was more pronounced for deformed nuclei; and it was speculated [3] that the source of difficulty might lie in the use of a spherical optical-model potential to describe the neutron scattering channels.

3. ANALYSIS

3.1. Trial calculations

Studies were carried out for a few nuclei in an attempt to reconcile theory and experiment by modifying ingredients of the calculation other than the form of the γ-ray penetrabilities. Some of these results are illustrated here, principally by calculations made for Au(n, γ); the data shown are those presented in the previous paper (CN-26/43). For convenience, the (n, γn') process was not included in these calculations at energies where it changes the gold capture cross section by $\leq 10\%$. The statistical-model calculations were made with a version [10] of the code NEARREX [8] and were verified to agree with sample calculations made with similar programs in use at four other laboratories. Several optical-model codes were used and intercompared.

The effects of width-fluctuation correlations were examined by varying the parameter Q_α from 0 to 2 (as T_α permits) and also by setting $F_{\alpha\beta} = 1$ to eliminate the width-fluctuation correction. Varying Q_α was determined to have no appreciable effect in the capture calculations. Eliminating the width-fluctuation correction increases the capture cross section almost uniformly by about 20% at energies below the first threshold for inelastic scattering and has little effect above the threshold. This, however, does not remove the discrepancy in the slope of the excitation function. The change produced is much too small, and for some nuclei (see below) the discrepancy can be observed below the first (n, n') threshold. The rest of the calculations discussed here include the correction for width fluctuations and use $Q_\alpha = 0$.

Results of calculations made with different sets [6, 11, 12] of optical-model parameters for the neutron elastic and inelastic scattering channels are shown in Fig. 2. The calculations were normalised by adjusting $T_\gamma(U_0)$ to produce agreement with the data at $E_n = 10$ keV. The values of $T_\gamma(U_0)$ varied $\sim \pm 20\%$ with the choice of optical potential and were in fair agreement (20-30%) with values of $\langle \Gamma_\gamma \rangle / D_{obs}$ deduced from

s-wave resonance parameters. As can be seen in Fig. 2, the relative cross sections calculated with the different potentials agree within ~ 20% from 10-700 keV.

Possible changes in the excitation function produced by using a non-spherical optical-model potential were investigated by making coupled-channel calculations [13] of the neutron scattering amplitudes. Generalised transmission coefficients were then obtained from the scattering amplitudes in the manner indicated in Ref. [4]. Coupled-channel calculations were made with the code described in Ref. [14] for ^{197}Au+n including the first five positive-parity states in ^{197}Au. The four excited states $1/2^+ - 7/2^+$ were assumed to result from coupling the $d_{3/2}$ valence proton to a one-quadrupole-phonon vibration of the core with a typical deformation parameter [13] of $\beta_2 = 0.2$. Coupled-channel calculations were also made for the tungsten isotopes $^{182, 183, 184, 186}$W assuming a quadrupole deformation of strength $\beta_2 = 0.24$. The $0^+ - 2^+ - 4^+$ states were included for the even isotopes, and the ground-state band $1/2^- - 7/2^-$ was used for ^{183}W. Capture calculations were then made with these generalised transmission coefficients together with the usual transmission coefficients (obtained from a spherical potential) for any other open (n, n') channels. The capture calculations were essentially identical for generalised transmission coefficients obtained with "complex coupling", for which both real and imaginary parts of the optical potential are deformed [13], and "real coupling" where only the real part of the potential is allowed to contribute to the nonspherical interaction.

Results of capture calculations for gold and natural tungsten using the spherical and nonspherical optical potentials are shown in Fig. 3. The two results are essentially identical for both the vibrational nucleus Au and the rotational nucleus W. Although the nonspherical treatment for W changes the transmission coefficients considerably at the higher incident energies, the capture calculation is still largely unaffected. This can be understood as an approximate cancellation of the differences in transmission coefficients in the quantities $\langle\theta_{\mu a}\rangle/\langle\theta_{\mu}\rangle$.

It was thus found unlikely that the discrepancy in the shape of the capture excitation function could be attributed to the neutron channels, and the exit-channel parameters were then examined. In its present form (Eqs. 3 and 4), the energy dependence of the γ-ray penetrabilities is determined by the energy and angular-momentum dependence of the level density. Capture calculations were made using the composite level density of Gilbert and Cameron[7], a simple Fermi-gas form $\rho \propto \exp(4aU)^{\frac{1}{2}}$, and a constant-temperature model $\rho \propto \exp(U/T)$. For values of the parameters $\underline{a}$ and T given in Ref. [7], these three representations produce negligible differences in the cross section at neutron energies below 1 MeV. A pairing correction [7] was used in the Fermi-gas formula, but this also has a small effect. Figure 4 illustrates that, to force the calculation to fit the general shape of the excitation function for gold up to ~ 700 keV, the inverse-temperature parameter $\underline{a}$ must take a value about

one order of magnitude different from the expected value of 18 MeV^{-1}. The spin dependence of the level density also changes the shape of the excitation function, since higher-energy neutrons bring more angular momentum into the compound nucleus. The spin dependence is represented here by $\rho(J) \propto [f(J) - f(J+1)]$, where $f(x) = \exp(-x^2/2\sigma^2)$; and the parameter σ is taken from Ref. [7]. Qualitiative agreement with a few (but not all) of the exitation functions could be produced by eliminating the spin dependence altogether. None of these gross changes in the level-density representation is attractive.

The calculations in which the spin dependence of the level density was varied can also be interpreted as introducing a spin dependence of the total radiation width, since the capture calculation depends only on the ratio $<\Gamma_\gamma>/D_{J\pi}$. Thus, the limited agreement mentioned above could also have been achieved using a standard [7] level density but a total radiation width which had the spin dependence $[f(J) - f(J+1)]^{-1}$ or, approximately, $(2J+1)^{-1}$. There is no evidence of such a dependence from neutron resonance-parameter studies. Calculations were also made with an arbitrary dependence of the total radiation width on the parity of the initial compound state. For gold, the p-wave contribution to the capture cross section dominates the s- and d-wave components in the region 60-600 keV, and the observed excitation function there could be reproduced by using a constant value of $(\Gamma_\gamma^+/\Gamma_\gamma^-)$ other than unity and by adjusting Γ_γ^+ to also produce agreement at 10 keV. However, a fit could only be achieved with the very unlikely [15] ratio $(\Gamma_\gamma^+/\Gamma_\gamma^-) \sim 5$.

3.2. Results for several nuclei

Standard calculations (as described in Section 2) were then carried out systematically for the eight data sets presented in the previous paper and also for ten excitation functions measured by Stupegia et al. [3] which also span the energy region of interest. The optical-model parameters were taken from Ref. [6], the level-density parameters from Ref. [7], and the $(n, \gamma n')$ process was included. The calculations were normalised by adjusting $T_\gamma(U_0)$ to approximately reproduce the data at the lowest energies. The normalisation is not critical for our present purposes since the shape of the exitation function changes little with wide variations in $T_\gamma(U_0)$. For ^{238}U, the fission competition was represented in the manner of Ref. [16] and is very small at energies below one MeV. The results are shown by the solid curves in Figs. 5 and 6. Within uncertainties in the data and reasonable variations of the parameters, we conclude that the standard treatment produces fairly good agreement with the capture data for Rh, Ta and Re but that a persistent discrepancy, of varying magnitude but always in the same direction, can be seen in the excitation functions for all the nuclei examined. The discrepancy can be observed in regions where there are no open (n, n') channels, e.g. in $^{89}Y(n, \gamma)$ below 1 MeV. The agreement is exceptionally poor for ^{98}Mo, ^{158}Gd, natural Gd, ^{170}Er, ^{176}Yb and natural W. We find no consistent variation of the magnitude of the discrepancy for different nuclei with

such properties as $\langle\Gamma_\gamma(U_0)\rangle$, $D(U_0)$, $\langle\Gamma_\gamma(U_0)\rangle/D(U_0)$, U_0, even or odd A, characteristics of measured capture γ-ray energy spectra, extrema in the s- and p-wave neutron strength functions, or the ground-state quadrupole deformation parameter.

Some additional calculations are shown in Figs. 5 and 6 to illustrate the degree of disagreement with the present theory. The broken curves were calculated with a much more slowly-varying γ-ray penetrability which has the empirical form $T_\gamma = C(U-\Delta)^m[f(J) - f(J+1)]$, where Δ is the pairing energy [7] and where the constant C was adjusted to produce the same value of $T_\gamma(U_0)$ used in the standard calculation. The exponent m is a measure of the energy dependence of T_γ required to roughly fit the shape of the excitation function below 1 MeV. If we retain Eq. (3) and a conventional level-density expression, then m is a measure of the energy variation of $\langle\Gamma_\gamma\rangle \propto T_\gamma(U)/\rho(U)$. For Au(n, γ) using the level density of Ref. [7], the value of $\langle\Gamma_\gamma(U)\rangle/\langle\Gamma_\gamma(U_0)\rangle$ calculated conventionally is about 1.2 at E_n = 700 keV, whereas it drops to about 0.6 for the empirical expression with m = 6.

4. CONCLUSIONS

The current statistical-model treatment of fast-neutron capture cross sections with parameters presently deemed reasonable does not reproduce the majority of the excitation functions examined. Even when normalised to data at energies up to 100 keV, the excitation functions calculated for some nuclei differ from the data by a factor of two at only 500 keV; and the discrepancy is always in the same direction. On phenomenological grounds, the most likely source of difficulty lies with the excitation-energy dependence of the γ-ray penetrability (or radiative strength function). Since there is no compelling reason to abandon Eq. (3) for the cases examined, and since such enormous departures from conventional level-density descriptions would otherwise be required to fit many of the cross sections with the standard calculation of $\langle\Gamma_\gamma(U)\rangle$, it is tempting to speculate that the difficulty lies with the traditional estimate [2] of the excitation-energy dependence of the partial radiation widths. Although this estimate is obtained from very simple assumptions about the electromagnetic matrix elements and the distribution of single-particle strength at high excitation energies, it is still difficult to understand how the estimate could be so grossly incorrect. It thus seems clear that new, fundamental work on the capture mechanism will be required before theory can be applied with confidence to fill gaps in the data for capture cross sections at neutron energies ~100 keV - 1 MeV.

REFERENCES

[1] Margolis, B., Phys. Rev. 88 (1952) 327.

[2] Blatt, J. M., and Weisskopf, V. F., Theoretical Nuclear Physics, Wiley, New York (1952).

[3] Stupegia, D. C., et al., J. Nucl. Energy 22 (1968) 267.

[4] Fricke, M. P., and Lopez, W. M., Phys. Letters 29B (1969) 393.

[5] Moldauer, P. A., Rev. Mod. Phys. 36 (1964) 1079; Phys. Rev. 135 (1964) B642; Phys. Rev. 171 (1968) 1164.

[6] Moldauer, P. A., Nucl. Phys. 47 (1963) 65.

[7] Gilbert, A., and Cameron, A. G. W., Can. J. Phys. 43 (1965) 1446.

[8] Moldauer, P. A., et al., Argonne National Laboratory Report ANL-6978 (1964).

[9] Moldauer, P. A., Proc. Conf. on Neutron Cross Section Technology, 1966, Washington, D. C., p. 163.

[10] Dunford, C. L., Atomics International Report NAA-SR-MEMO 12530 (1967).

[11] Lister, D., et al., Phys. Rev. 162 (1967) 1077.

[12] Perey, F. G., and Kinney, W. E., Oak Ridge National Laboratory Report ORNL-TM-2159 (1968).

[13] Tamura, T., Rev. Mod. Phys. 37 (1965) 679.

[14] Tamura, T., Oak Ridge National Laboratory Report ORNL-4152 (1967).

[15] Cameron, A. G. W., Proc. Conf. on the Neutron Interactions with the Nucleus, Columbia Univ., 1957, USAEC Report TID-7547.

[16] Dunford, C. L., "Evaluation of Heavy Even-Even Nuclide Elastic and Inelastic Cross-Sections by Means of a Non-spherical Optical Model," Nuclear Data for Reactors (Paris Conf., 1966), IAEA, Vienna (1967).

FIGURE CAPTIONS

Fig. 1. Statistical-model calculations of the average capture cross section for gold. In the region spanned by the bracket labeled $T_\gamma(U)$, the competition from inelastic scattering can be treated rigorously for each level in ^{197}Au, and the effect of the $(n, \gamma n')$ process is small. Below this region T_γ is approximately constant since the compound excitation energy $U = U_0 + E_n$ differs little from the binding energy U_0.

Fig. 2. Capture cross sections for gold calculated with different optical-model parameters. The solid curve was calculated with the parameters of Ref. [6], the long-dash curve with Ref. [12], and the short-dash curve with Ref. [11].

Fig. 3. Capture cross sections calculated with neutron transmission coefficients obtained from spherical and nonspherical optical-model potentials. A vibrational model was assumed for Au and a rotational model for W.

Fig. 4. Capture cross sections for gold calculated with a reasonable value (18 MeV^{-1}) of the level-density parameter $\underline{a}$ and with lower values required to force agreement with the data.

Fig. 5. Capture cross-section data of paper CN-26/43 vs. statistical-model calculations. The solid curves were obtained with the standard theory and the broken curves with γ-ray penetrabilities proportional to a power m of the compound excitation energy.

Fig. 6. Capture cross-section data of Ref. [3] vs. statistical-model calculations. As in Fig. 5 the solid curves are standard calculations, and the broken curves use $T_\gamma \propto U^m$.

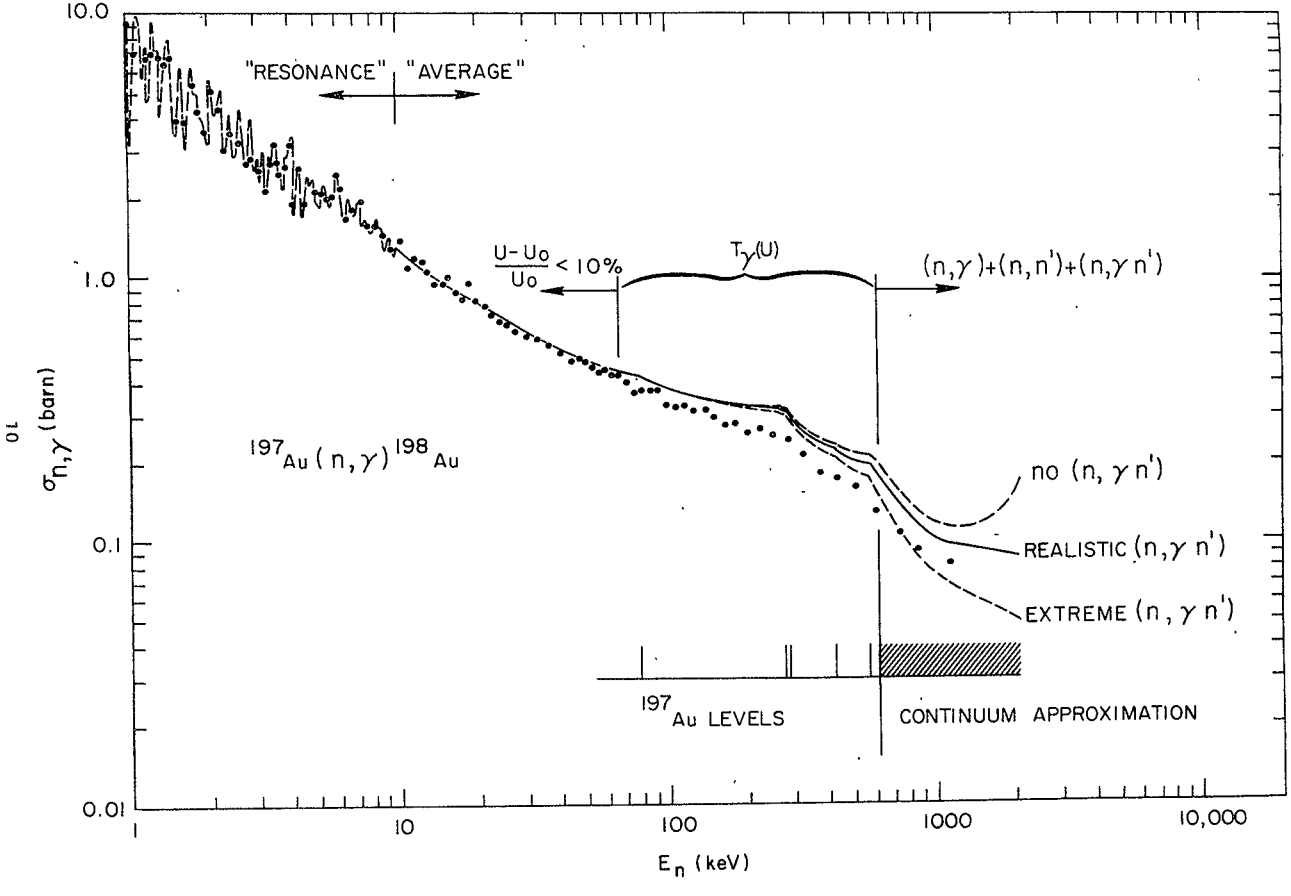
10.0
1.0
0.1
0.01
"RESONANCE"
"AVERAGE"
$\frac{U-U_0}{U_0} < 10\%$
$T_\gamma(U)$
$(n,\gamma)+(n,n')+(n,\gamma n')$
$^{197}Au(n,\gamma)^{198}Au$
no $(n,\gamma n')$
REALISTIC $(n,\gamma n')$
EXTREME $(n,\gamma n')$
^{197}Au LEVELS
CONTINUUM APPROXIMATION
$\sigma_{n,\gamma}$ (barn)
1
10
100
1000
10,000
E_n (keV)

Figure 1

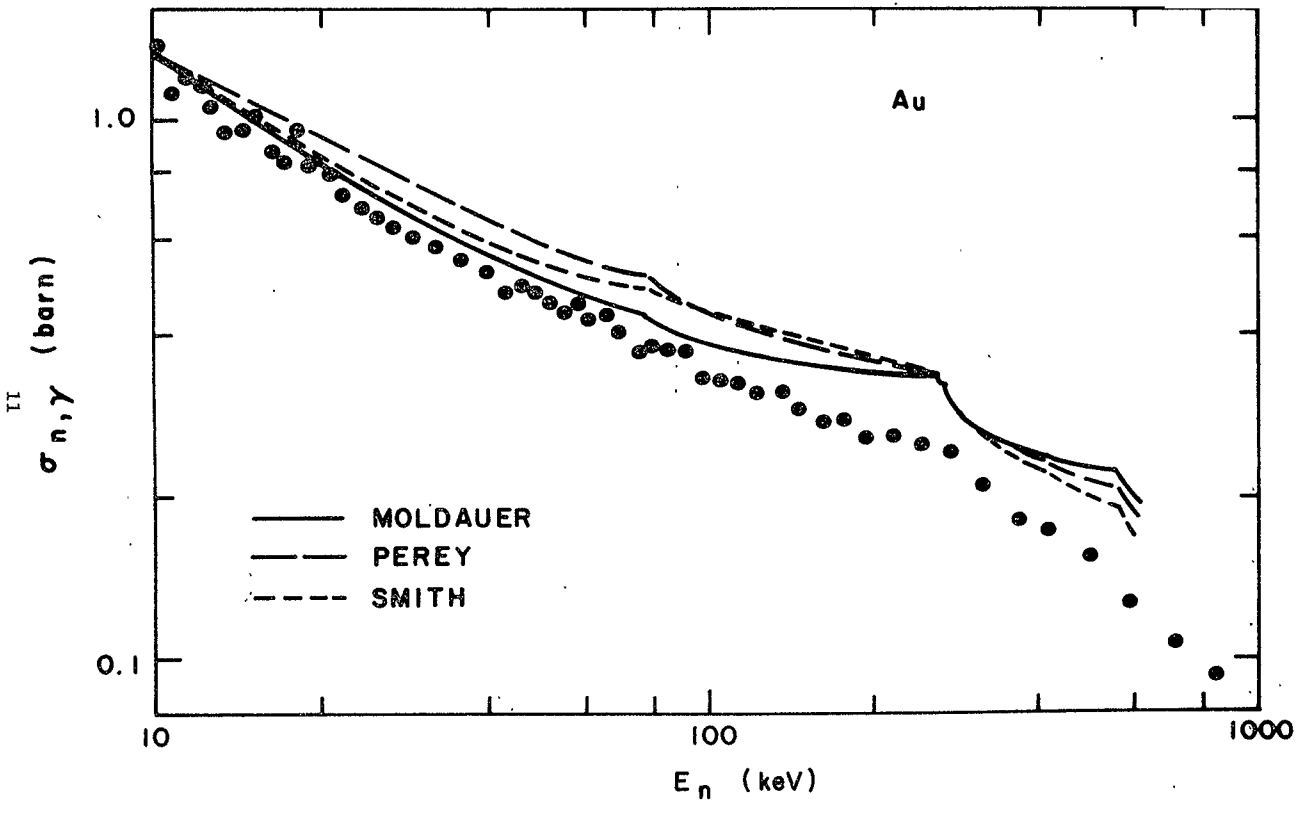
Au
1.0
0.1
10
100
1000
$\sigma_{n,\gamma}$ (barn)
E_n (keV)
MOLDAUER
PEREY
SMITH

Figure 2

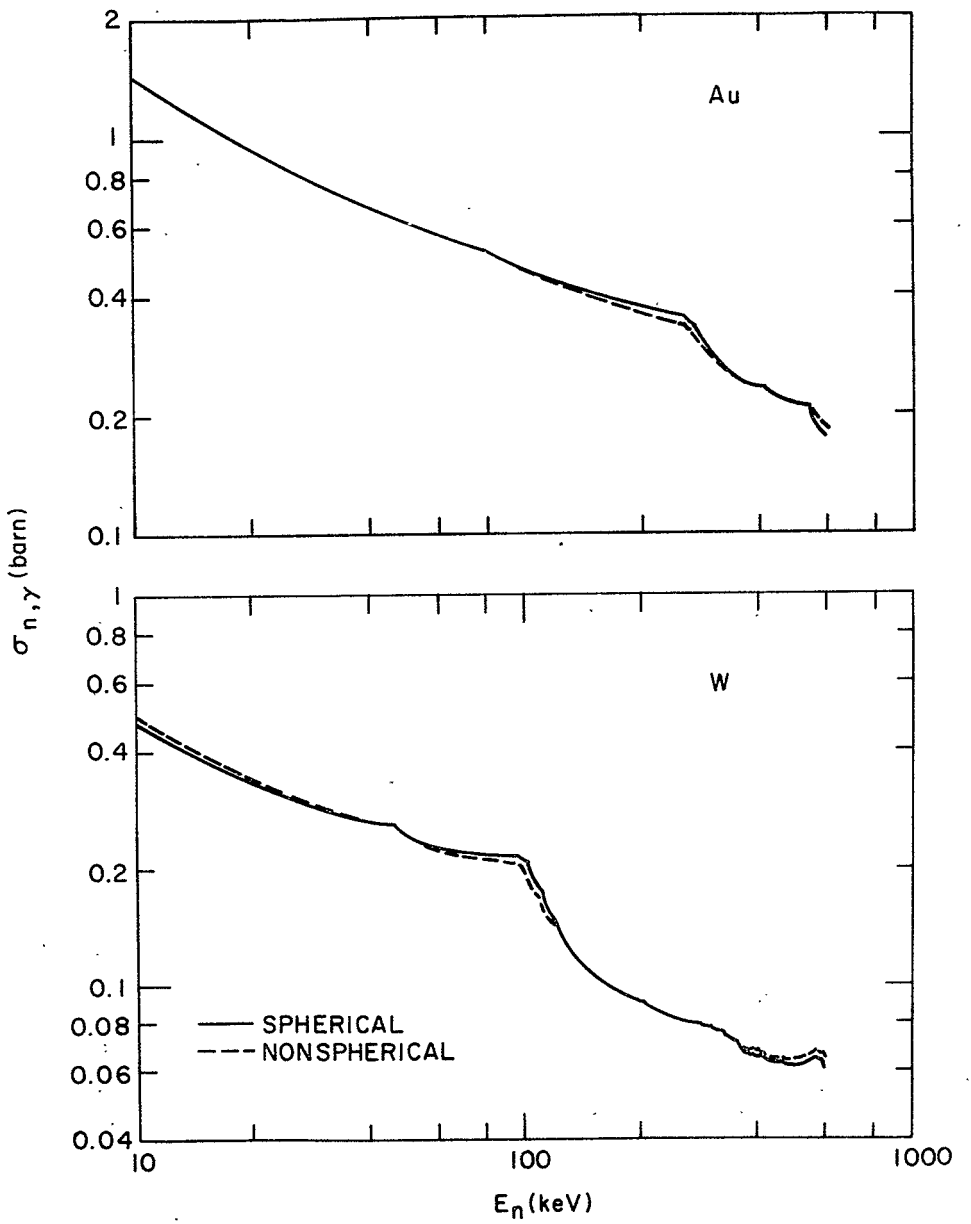
Au
W
SPHERICAL
NONSPHERICAL
$\sigma_{n,\gamma}$ (barn)
E_n(keV)
2
1
0.8
0.6
0.4
0.2
0.1
0.08
0.06
0.04
10
100
1000

Figure 3

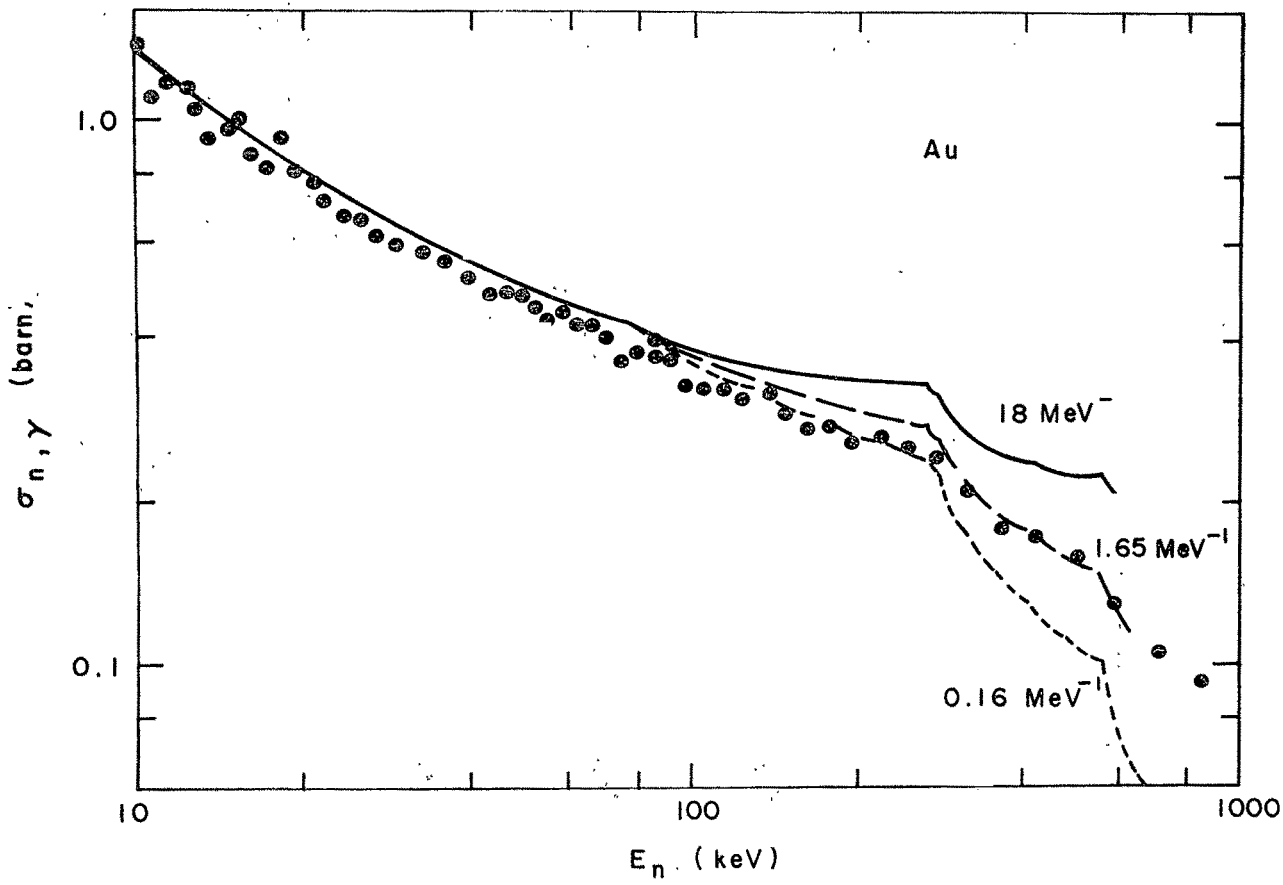
1.0
0.1
Au
18 MeV⁻¹
1.65 MeV⁻¹
0.16 MeV⁻¹
10
100
1000
$\sigma_{n,\gamma}$ (barn)
E_n (keV)

Figure 4

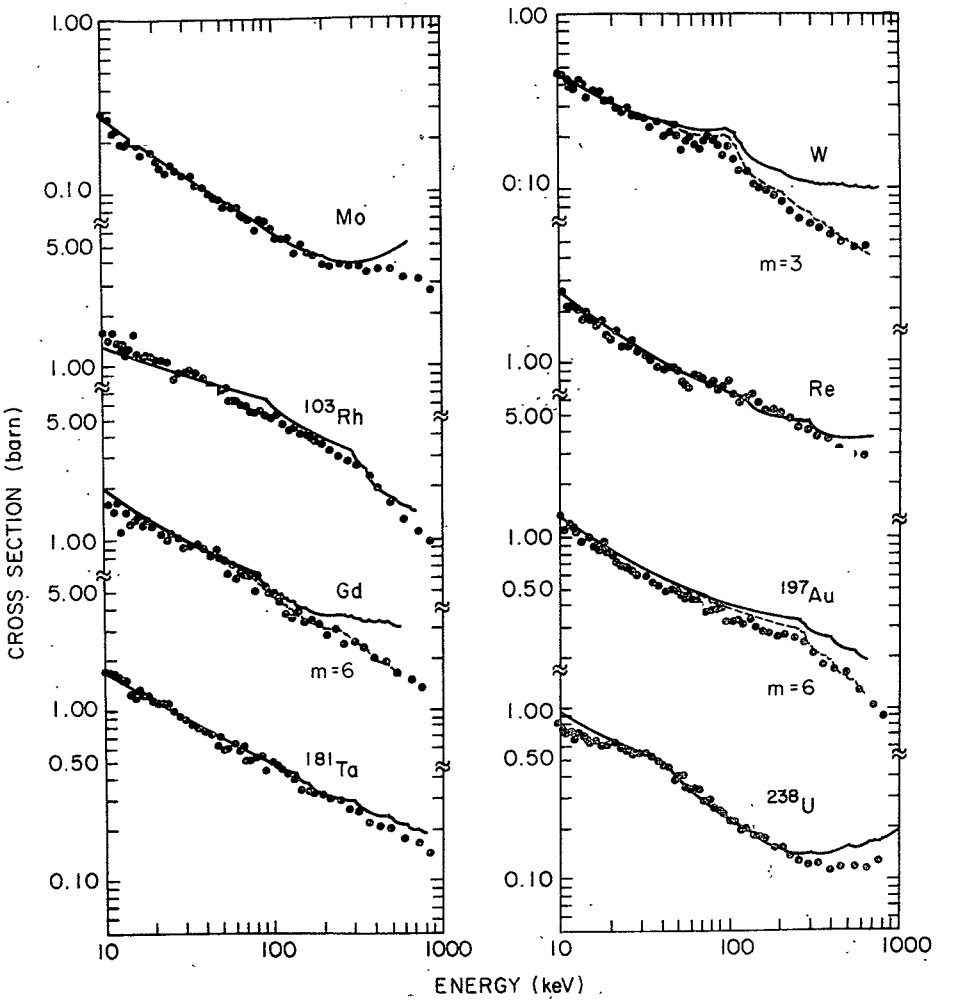
CROSS SECTION (barn)
ENERGY (keV)
Mo
103Rh
Gd
m=6
181Ta
W
m=3
Re
197Au
m=6
238U
1.00
0.10
5.00
1.00
5.00
1.00
5.00
1.00
0.50
0.10
1.00
0.10
5.00
1.00
5.00
1.00
0.50
1.00
0.50
0.10
10
100
1000
10
100
1000

Figure 5

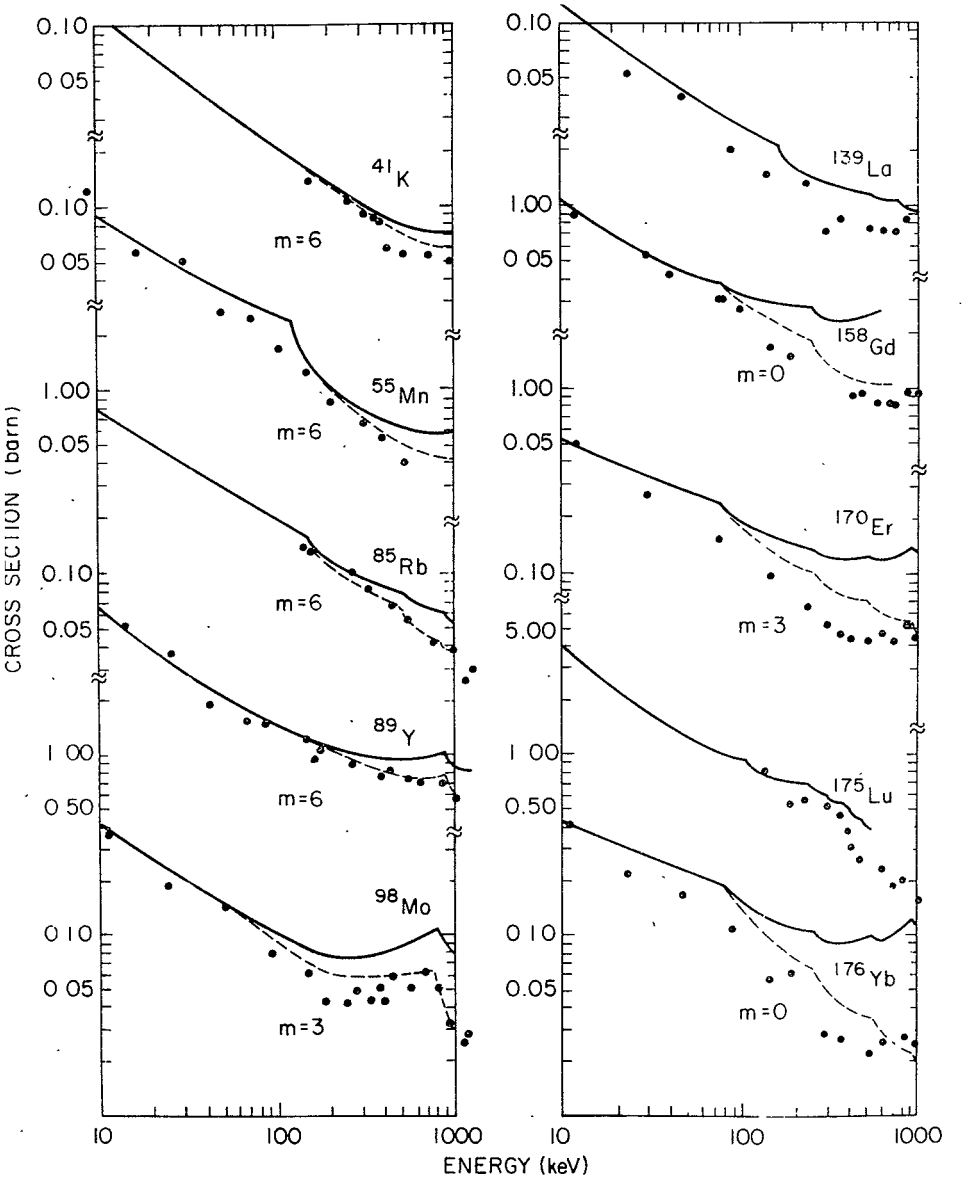
CROSS SECTION (barn)
ENERGY (keV)
41K
m=6
55Mn
m=6
85Rb
m=6
89Y
m=6
98Mo
m=3
139La
158Gd
m=0
170Er
m=3
175Lu
176Yb
m=0

Figure 6

NASA DISTRIBUTION LIST

NASA Lewis Research Center
21000 Brookpark Road
Cleveland, Ohio 44135

	Name	No. of Copies	Mail Stop
Attention:	Sam Barile	10	49-2
	Dr. Bernard Lubarsky	1	3-3
	John E. Dilley	1	500-309
	Technology Utiliz. Office	1	3-19
	Library	2	60-3
	Report Control Office	1	5-5
	Donald Bogart	1	49-2
	Donald F. Shook	1	49-2
	John C. Liwosz	1	49-2
	Vincent F. Hlavin	1	3-14

NASA Scientific and Technical Information Facility — 1
Box 5700
Bethesda, Maryland 20014

NASA Ames Research Center — 1
Moffett Field, California 94035
Attention: Library

NASA Flight Research Center — 1
P. O. Box 273
Edwards, California 93523
Attention: Library

NASA Goddard Space Flight Center — 1
Greenbelt, Maryland 20771
Attention: Library

NASA Langley Research Center — 1
Langley Station
Hampton, Virginia 23365
Attention: Library

NASA Manned Spacecraft Center — 1
Houston, Texas 77001
Attention: Library

No. of Copies

NASA Marshall Space Flight Center
Huntsville, Alabama 35812
Attention: Library

Jet Propulsion Laboratory 1
4800 Oak Grove Drive
Pasadena, California 91103
Attention: Library

National Aeronautics and Space 1
Administration
Washington, D. C. 20546
Attention: RR/Research Division

National Aeronautics and Space 1
Administration
Washington, D. C. 20546
Attention: RN/Space Power and Electric
Propulsion Division

NASA Electronics Research Center 1
575 Technology Square
Cambridge, Massachusetts 02139
Attention: Dr. Alfredo G. Kniazzeh

U. S. Atomic Energy Commission 1
Technical Reports Library
Washington, D. C. 20545

U. S. Atomic Energy Commission
Technical Information Service Center
P. O. Box 62
Oak Ridge, Tennessee 37830

CONTRACTOR'S DISTRIBUTION LIST

Los Alamos Scientific Laboratory 2
P. O. Box 1663
Los Alamos, New Mexico
Attention: Dr. L. Stewart
Dr. B. C. Diven

	No. of Copies
Oak Ridge National Laboratory P. O. Box X Oak Ridge, Tennessee 37830 Attention: Dr. R. L. Macklin Dr. L. W. Weston Dr. R. Gwin Dr. J. H. Gibbons	4
Rensselaer Polytechnic Institute Department of Nuclear Engineering and Science Troy, New York 12181 Attention: Prof. R. C. Block	1
Argonne National Laboratory 9700 South Cass Avenue Argonne, Illinois 60439 Attention: Dr. D. C. Stupegia Dr. W. P. Poenitz Dr. P. A. Moldauer Dr. S. A. Cox	4
Institut für Angewandte Kernphysik Ges. für Kernforschung Karlsruhe Karlsruhe, Germany Attention: Dr. F. H. Fröhner	1
Institut für Neutronenphysik und Reaktortechnik Ges. für Kernforschung Karlsruhe Karlsruhe, Germany Attention: Dr. J. J. Schmidt	1
Atomic Weapons Research Establishment Aldermaston, Berkshire, England Attention: Dr. J. B. Parker Dr. P. H. White	2
National Neutron Cross Section Center Brookhaven National Laboratory Associated Universities, Inc. Upton, New York Attention: Dr. M. D. Goldberg	1

	No. of Copies
Research Establishment Risö Roskilde, Denmark Attention: Dr. J. Als-Nielsen	1
Research Institute of National Defense Stockholm, Sweden Attention" Dr. I. Bergqvist	1
Gulf General Atomic Incorporated Accelerator Physics Department P. O. Box 608 San Diego, California 92112 Attention: Dr. M. P. Fricke	20